Polymer Chemistry

Accepted Manuscript

This is an *Accepted Manuscript*, which has been through the Royal Society of Chemistry peer review process and has been accepted for publication.

Accepted Manuscripts are published online shortly after acceptance, before technical editing, formatting and proof reading. Using this free service, authors can make their results available to the community, in citable form, before we publish the edited article. We will replace this *Accepted Manuscript* with the edited and formatted *Advance Article* as soon as it is available.

You can find more information about *Accepted Manuscripts* in the Information for Authors.

Please note that technical editing may introduce minor changes to the text and/or graphics, which may alter content. The journal's standard Terms & Conditions and the Ethical guidelines still apply. In no event shall the Royal Society of Chemistry be held responsible for any errors or omissions in this *Accepted Manuscript* or any consequences arising from the use of any information it contains.

ROYAL SOCIETY OF CHEMISTRY

www.rsc.org/polymers

Cite this: DOI: 10.1039/c0xx00000x

www.rsc.org/xxxxxx

PAPER

Multifunctional ATRP based pH Responsive Polymeric Nanoparticles for Improved Doxorubicin Chemotherapy in Breast Cancer by Proton Sponge Effect/Endo-Lysosomal Escape

Shantanu V. Lale, [a,b] Arun Kumar, [a,b] Farhat Naz, [c] Alok C. Bharti [d] and Veena Koul [*a,b]

Received (in XXX, XXX) Xth XXXXXXXXX 20XX, Accepted Xth XXXXXXXXX 20XX
DOI: 10.1039/b000000x

Folic acid and trastuzumab functionalized pH responsive biodegradable polymeric nanosystem comprising of poly(dimethylaminoethyl methacrylate)-poly(polyethylene glycol methacrylate)-poly(caprolactone)-poly(polyethylene glycol methacrylate)-poly(dimethylaminoethyl methacrylate) [PDMAEMA-PPEGMA-PCL-PPEGMA-PDMAEMA] was designed and developed for improving chemotherapeutic efficacy of doxorubicin while minimizing its cardiotoxicity in breast cancer therapy. The nanosystem consists of multiple polyethylene glycol chains which impart stealth nature to the nanoparticles. Polymer-doxorubicin conjugate via acid responsive hydrazone linkage resulted in enhanced doxorubicin release (~89%) in endo-lysosomal pH as compared to that in physiological pH (~29%). Nanoparticles also exhibited proton sponge effect leading to endo-lysosomal escape of nanoparticles which resulted in minimal drug degradation and faster drug action. Folic acid and trastuzumab were incorporated in the nanosystem to selectively target breast cancer cells. *In vitro* and *in vivo* studies in breast cancer cell lines and Ehrlich ascites tumor bearing Swiss albino mice showed enhanced cellular uptake and improved therapeutic efficacy of the nanosystem with nanoparticles achieving ~92% tumor regression as compared to ~36% tumor regression observed with free doxorubicin. This enhanced therapeutic efficacy was achieved with minimal cardiotoxicity as observed in histopathology and blood biochemistry. The findings highlight the potential of the nanosystem in chemotherapeutic management of breast cancer with its high therapeutic efficacy and minimal cardiotoxicity.

Introduction

Polymer nanoparticles (NPs) for doxorubicin delivery in breast cancer have been investigated by many researchers to overcome cardiotoxicity, non-specificity and acquired resistance of cancer cells to current doxorubicin chemotherapy.[1-3] Polymeric nanoparticles help to improve bioavailability of doxorubicin by passive targeting of tumors via enhanced permeation and retention (EPR) effect, by increasing circulation half life of doxorubicin and by overcoming acquired cancer cell resistance.[4] These polymeric nanosystems suffer from few drawbacks which lead to decreased antitumor efficacy of doxorubicin. Doxorubicin hydrochloride is a water soluble drug which makes it difficult to physically load doxorubicin in nanoparticles in sufficient amount. Doxorubicin leakage/release from the encapsulated nanoparticles can occur during circulation which results in non-specific action of doxorubicin on normal healthy cells, thus defeating the purpose of using nanoparticles for doxorubicin delivery.[5] Also, passively targeted nanoparticles generally exhibit limited cancer targeting ability as compared to active targeted nanoparticles leading to low doxorubicin bioavailability at tumor site which results in lower therapeutic efficacy.[6]

Polymer-doxorubicin conjugates have been developed to overcome these shortcomings. Doxorubicin covalently binds with the polymer via a spacer which prevents doxorubicin release/leakage during nanoparticle circulation while facilitating doxorubicin delivery in specific target tissue.[7, 8] Several researchers have reported polymer-doxorubicin conjugates with pH sensitive linkages like acetal, ketal, hydrazone and cis-aconityl.[9-13] Hydrazone linkage for doxorubicin conjugation with the polymer is widely investigated since it is stable in physiological pH whereas in endocytic compartment of cancer cells, the linkage breaks leading to release of doxorubicin. Thus, doxorubicin will be specifically released at the tumor site enhancing its bioavailability while minimizing side effects. Doxorubicin conjugation with the polymer also enhances total drug content/payload in the resulting polymeric nanoparticles.[14]

Many synthetic polymers have been investigated for polymer-doxorubicin conjugates for cancer therapeutics.[15-17] Most of them are non-biodegradable in nature, thus limiting their use in clinical settings. Polycaprolactone and polyethylene glycol (PEG) polymers are biodegradable polymers approved by US FDA for drug delivery applications.[18, 19] Unlike many non-biodegradable polymers used in drug delivery applications, nanoparticles based on polycaprolactone-polyethylene glycol do not accumulate in the body and are easily removed from the body due to their

biodegradable nature.[20, 21]

Synthesizing polymers of predetermined molecular weight with narrow molecular weight distribution is very essential in drug delivery applications. Atom transfer radical polymerization (ATRP), a living polymerization technique, is widely used to synthesize polymers of predetermined molecular weight with low polydispersity.[22] It also allows synthesis of copolymers with multiple PEG chains, which can be further conjugated with doxorubicin molecules leading to increased doxorubicin content of the resulting polymeric nanoparticles.[14]

Therapeutic efficacy of the polymer-doxorubicin conjugates can be significantly improved by cancer cell specific targeting of nanoparticles. Various ligands like aptamer, folic acid, antibodies, growth factors, hormones, sugars etc. have been extensively studied for their efficacy in active targeting of cancer cells.[23-27] Folic acid is widely used as a ligand for targeting cancer cells since cancer cells over-express folate receptor RFα (which is minimally expressed in normal healthy cells) to fulfil increased requirement of folic acid for DNA synthesis and faster multiplication. RFα folate receptor shows high binding affinity toward folic acid (K_d < 1 nM), making folic acid an attractive targeting ligand for active targeting of cancer cells.[28] Trastuzumab (Herceptin®) is a humanized monoclonal antibody specific for human epidermal growth factor receptor 2 (EGFR2/HER2 receptor). It has high binding affinity toward HER2 receptors (K_d = 0.1 nM) making it an excellent ligand for precisely targeting breast cancer cells which express HER2 receptors.[29]

In the present work, folate and trastuzumab functionalized biodegradable multifunctional polymeric nanosystem was developed for targeted doxorubicin delivery in breast cancer (Scheme 1). ATRP based PDMAEMA-PPEGMA-PCL-PPEGMA-PDMAEMA copolymer was synthesized with desired molecular weight and low polydispersity. It consists of multiple PEG chains which impart stealth nature to the NPs, thereby enhancing their circulation half life. Dimethylaminoethyl groups induce proton sponge effect resulting in endo-lysosomal escape of NPs causing faster drug release in cancer cells. To prevent leakage/release of doxorubicin from NPs during circulation and to improve doxorubicin content of NPs, doxorubicin molecules were conjugated on PEG chains of the polymer through acid responsive hydrazone linkage. To selectively target cancer cells and to enhance the cellular uptake of NPs, folate and trastuzumab were incorporated in the nanosystem. Nanoparticles were evaluated for biocompatibility, hemocompatibility, drug release and endosomolytic behavior. Antitumor efficacy of multifunctional doxorubicin conjugated polymeric nanoparticles was evaluated in breast cancer cell lines and in Ehrlich ascites tumor bearing Swiss albino mice. Toxicity of NPs was studied using histopathology and serum biochemistry. All the studies were carried out to substantiate the superior therapeutic potential of our nanosystem in breast cancer therapy.

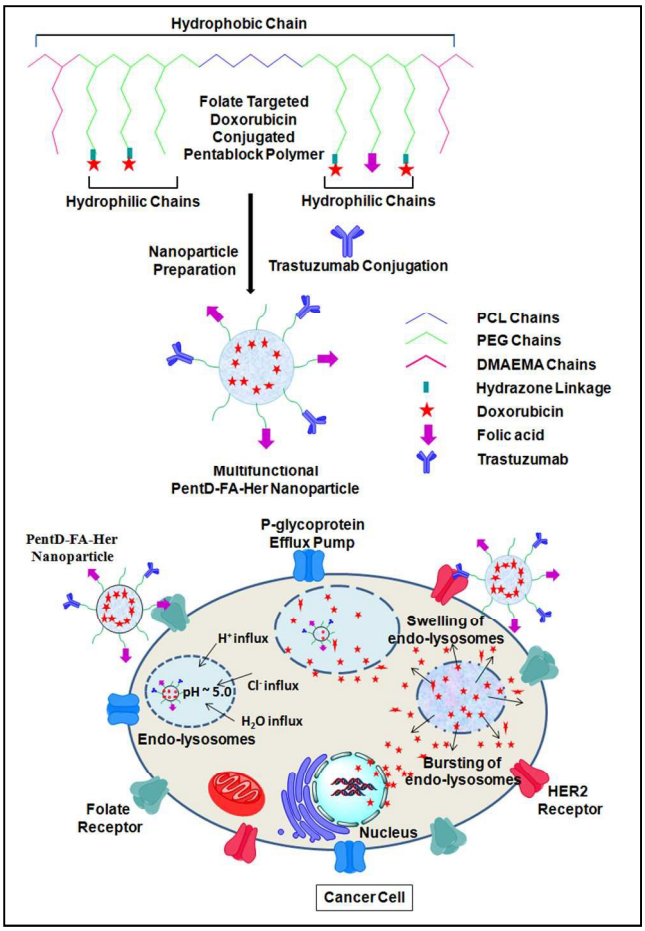

Scheme 1. Schematic representation of pH responsive PDMAEMA-PPEGMA-PCL-PPEGMA-PDMAEMA polymeric nanoparticles for improved doxorubicin chemotherapy in breast cancer

Experimental

Materials

Polycaprolactone diol (PCL) (M_n ~2000 Da), N,N,N′,N′,N″-pentamethyldiethylenetriamine (PMDETA), α-bromoisobutyryl bromide, folic acid, 4-dimethylaminopyridine (DMAP), N,N′-dicyclohexylcarbodiimide (DCC), N-hydroxysuccinimide (NHS), Pluronic F68, trehalose, 3-(4,5-dimethyl-2-thiazolyl)-2,5-diphenyl-tetrazolium bromide (MTT) were purchased from Sigma-Aldrich (St. Louis, MO, USA) and used as received without further purification. Copper (I) bromide [CuBr (I)] (Sigma-Aldrich) was purified before use by sequential washings of glacial acetic acid, ethanol and diethyl ether followed by vacuum drying. Poly(ethylene glycol) methacrylate (PEGMA) (M_n ~360 Da) and N,N-dimethylaminoethyl methacrylate (DMAEMA) (Sigma-Aldrich) were purified from polymerization inhibitor monomethyl ether hydroquinone (MEHQ) by passing through basic alumina column. The marketed product Herclon™ (Trastuzumab for Injection) (Roche, India) was purchased and purified before use by dialyzing in phosphate buffer saline pH 7.4 (PBS) to obtain pure trastuzumab. Doxorubicin was obtained as a gift sample from Ranbaxy Laboratories Ltd, New Delhi. Dulbecco's modified Eagle's medium (DMEM), fetal bovine serum (FBS) and penicillin-streptomycin solution were obtained from Cellclone, Genetix Biotech Ltd. (New Delhi, India).

Synthesis of PDMAEMA-PPEGMA-PCL-PPEGMA-PDMAEMA pentablock copolymer

Pentablock copolymer PDMAEMA-PPEGMA-PCL-PPEGMA-PDMAEMA was synthesized sequentially by first synthesizing PCL macroinitiator which, in the next step, initiated ATRP of PEGMA and DMAEMA to synthesize PDMAEMA-PPEGMA-PCL-PPEGMA-PDMAEMA as shown in Scheme 2.

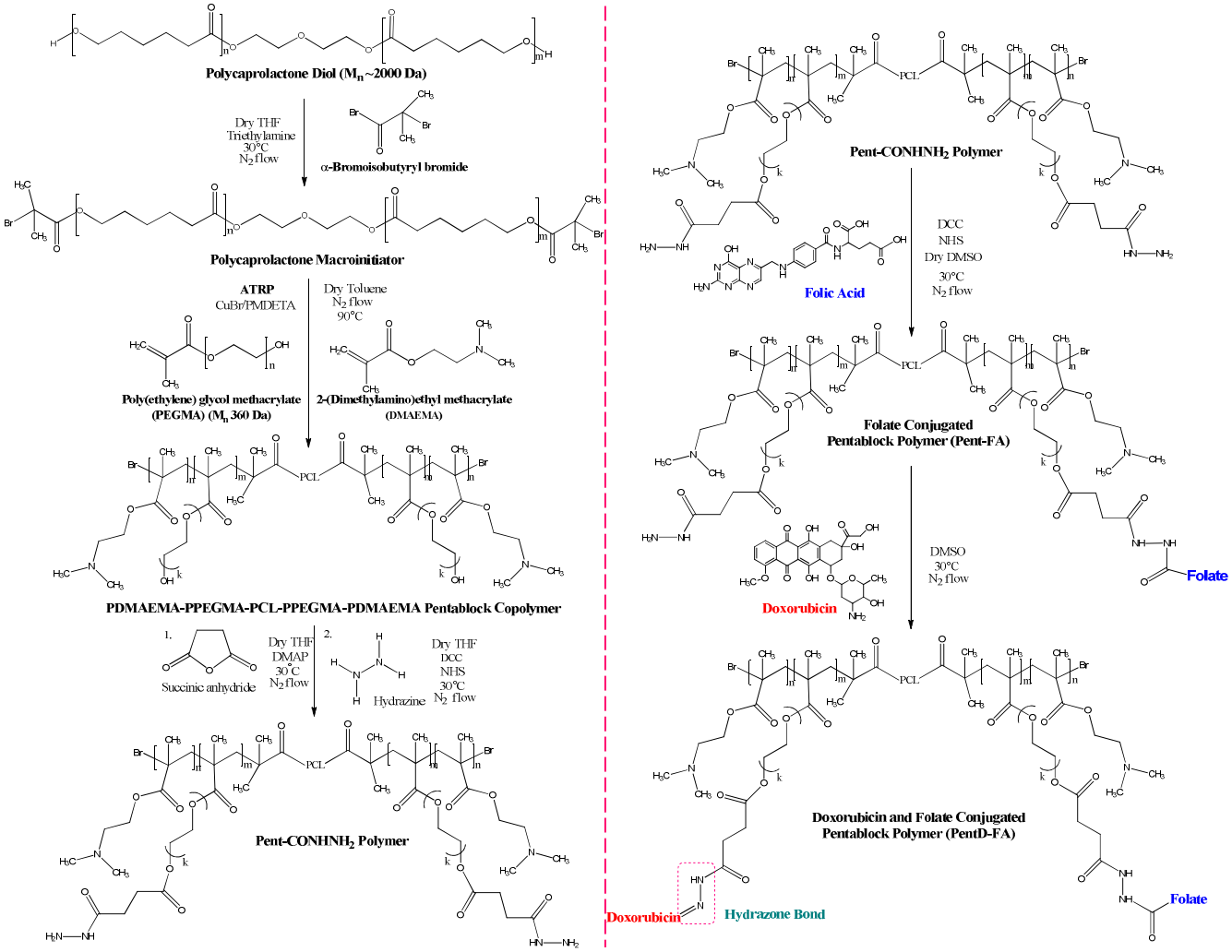

Scheme 2. Reaction scheme for synthesis of doxorubicin conjugated PDMAEMA-PPEGMA-PCL-PPEGMA-PDMAEMA pentablock copolymer

PCL macroinitiator synthesis

PCL diol (M_n ~2000 Da, 15.0 g; 7.5 mM) and dry triethylamine (5.22 mL; 37.5 mM) were dissolved in 50 mL dry THF in a Schlenk flask over ice bath for 30 min. α-Bromoisobutyryl bromide (4.64 mL; 37.5 mM) was then dropwise added to the cold solution over the period of 30 min and the reaction was continued for 24 h at 30 °C under N_2 atmosphere with continuous stirring. After 24 h, the mixture was filtered and evaporated in rotary evaporator (HB 10, Ika, Germany). The viscous solution obtained was extracted with dichloromethane (DCM) and saturated solution of $NaHCO_3$. DCM layer was then dried over Na_2SO_4 for 2 h and evaporated under vacuum. Resulting viscous solution was precipitated thrice in cold diethyl ether and dried under vacuum. PCL macroinitiator (PCL-Br) thus obtained was characterized by ^{1}H-NMR (300 MHz, Brukers, USA) and ATR-FTIR (Perkin Elmer, USA). Yield = 87%.

Synthesis of pentablock copolymer by ATRP of PEGMA and DMAEMA

Weighed amounts of CuBr (I) (0.43 g; 3 mM) and PMDETA (0.626 mL; 3 mM) were mixed with 30 mL dry toluene in a Schlenk tube and stirred for 1 h at 90 °C under N_2 atmosphere. PEGMA (M_n ~360 Da, 4.9 mL; 15 mM) was then added in the Schlenk flask followed by continuous nitrogen bubbling in the reaction mixture. PCL-Br (3.45 g; 1.5 mM) was further added and reaction was continued at 90 °C for 24 h under N_2 atmosphere. DMAEMA (1.01 mL; 6 mM) was further added to the mixture and reaction was continued for further 12 h. Then the reaction mixture was purified from copper complex by passing it through activated neutral alumina column. Eluate obtained was concentrated on rotary evaporator and precipitated thrice in cold diethyl ether followed by vacuum drying. PDMAEMA-PPEGMA-PCL-PPEGMA-PDMAEMA pentablock copolymer thus obtained was characterized by ^{1}H-NMR, ^{13}C-NMR (300 MHz, Brukers, USA), ATR-FTIR and gel permeation chromatography (GPC) (Waters, USA). Yield = 75%.

Conjugation of folic acid and doxorubicin with the pentablock copolymer

Out of eight hydroxyl groups of the pentablock polymer, six were sequentially converted to -$CONHNH_2$ for further conjugation with folic acid and doxorubicin, whereas remaining two hydroxyl groups were converted to -COOH for further conjugation with trastuzumab.

Functionalizing hydroxyl groups of pentablock polymer to -$CONHNH_2$

In Schlenk flask, pentablock polymer ($M_{n\ (NMR)}$ ~5800 Da, 5.0 g; 6.9 mM corresponding to eight hydroxyl groups) was dissolved in 50 mL dry THF along with succinic anhydride (1.38 g; 13.8 mM) and DMAP (0.345 g; 3.45 mM) and kept for stirring for 24 h at 30 ºC under N_2 atmosphere. Reaction mixture was then concentrated and precipitated thrice in cold diethyl ether followed by vacuum drying. Pentablock polymer with -COOH functionality (Pent-COOH) thus obtained was characterized by ^{1}H-NMR and ATR-FTIR. Yield = 84%.

Pent-COOH (4.0 g; 4.13 mM corresponding to six carboxyl groups) was then dissolved in 50 mL dry THF in a Schlenk flask followed by DCC (0.852 g; 4.13 mM) and NHS (0.475 g; 4.13 mM) and reaction mixture was stirred overnight at 30 ºC under N_2 atmosphere. Hydrazine hydrate (0.2 mL; 4.13 mM) was further added to the reaction mixture and reaction was continued for another 12 h. The reaction mixture was then purified by filtration to remove DCC by-product, concentrated and precipitated thrice in cold diethyl ether. Pentablock polymer containing -$CONHNH_2$ functionality (Pent-$CONHNH_2$) thus synthesized was characterized by ATR-FTIR. Yield = 83%.

Conjugation of folic acid with pentablock copolymer

In Schlenk flask, folic acid (0.53 g; 1.2 mM) was dissolved in 50 mL dry DMSO followed by DCC (0.497 g; 2.4 mM) and NHS (0.276 g; 2.4 mM) and the reaction mixture was stirred overnight at 30 ºC under N_2 atmosphere. Pent-$CONHNH_2$ (3.5 g; 1.2 mM corresponding to two -$CONHNH_2$ groups) was then added to the reaction mixture and reaction was continued for 24 h at 30 ºC under N_2 atmosphere. The reaction mixture was purified by filtering the DCC by-product, dialyzed and lyophilized. Yellow colored folate conjugated pentablock polymer (Pent-FA) thus obtained was characterized by ^{1}H-NMR, UV-Visible spectroscopy (Perkin Elmer, USA) and CHN analysis (Vario EL III Element Analyzer, Elementar Analysensysteme GmbH, Germany). Yield = 81%.

Doxorubicin conjugation with pentablock copolymer

In Schlenk flask, Pent-FA (1.0 g; 0.7 mM) and doxorubicin hydrochloride (0.375 g; 0.7 mM) were dissolved in 50 mL dry DMSO and reaction mixture was stirred in dark at 30 ºC for 72 h under N_2 atmosphere. Reaction mixture was further purified by dialysis to remove unconjugated doxorubicin and was lyophilized. Red colored folate and doxorubicin conjugated polymer (PentD-FA) thus synthesized was characterized by UV-Visible spectroscopy and differential scanning calorimetry (DSC). Thermal behavior of pentablock polymer, doxorubicin hydrochloride, physical mixture of doxorubicin and polymer; and doxorubicin conjugated polymer was analyzed by DSC (TA Q2000, TA Instruments, USA). Samples were scanned over a range of 0 - 300 °C with heating rate of 10 °C/min.

Similarly, doxorubicin conjugated polymer which lacks folic acid (PentD, non-targeted polymer), was synthesized by reacting Pent-$CONHNH_2$ polymer with doxorubicin hydrochloride. Yield = 79%.

Determination of doxorubicin content of conjugated polymers

Doxorubicin content of the doxorubicin conjugated polymers (PentD and PentD-FA) was quantified by breaking hydrazone linkage in acidic media to release doxorubicin molecules. Polymer (10 mg) was mixed with 10 mL of 0.1 N HCl followed by sonication for 5 min. It was stirred in the dark at 30 ºC for 48 h and then centrifuged at 25000 rpm for 10 min. Supernatant was analyzed at 481 nm using UV-Visible spectrophotometer and doxorubicin content was quantified using doxorubicin standard calibration curve.

Preparation and characterization of nanoparticles

Nanoparticles were prepared by nanoprecipitation method. Polymer solution in DMSO (5 mg/mL; 5 mL) was dropwise added using a syringe to 45 mL water with 1% Pluronic F68 under mild stirring at 30 ºC. The resulting nanoparticle suspension was purified by washing with water using Amicon ultracentrifugal filter (30 kDa) and then lyophilized with 10% trehalose as cryoprotectant.

Nanoparticles were characterized using dynamic light scattering (DLS) (Zetasizer Nano ZS, Malvern Instruments Ltd, UK), atomic force microscopy (AFM) (Nanoscope Multimode AFM, Digital Instruments, USA), scanning electron microscopy (SEM) (Zeiss EVO 50, Carl Zeiss Microscopy GmbH, Germany) and high-resolution transmission electron microscopy (HRTEM) (Technai G2, 200 kV, FEI, USA). Reconstitution time of the polymeric nanoparticles was determined using 10 mL water.

Trastuzumab conjugation on nanoparticles

Doxorubicin conjugated polymeric nanoparticles (PentD NPs and PentD-FA NPs) (10 mg/mL) were incubated with EDC (25 mg; 161 µM) and NHS (25 mg; 217 µM) at 4 °C for 30 min with slow stirring. Trastuzumab (3 mL; 1 mg/mL) was then incubated with nanoparticles for another 4 h at 4 °C with gentle stirring. Trastuzumab conjugated nanoparticles thus obtained (PentD-Her NPs and PentD-FA-Her NPs) were washed three times with water using Amicon ultracentrifugal filter, lyophilized and stored at 4 °C. Filtrate from each washing was analyzed by Biuret assay to determine unconjugated trastuzumab. Concentration of conjugated trastuzumab on nanoparticle surface was calculated by subtracting unconjugated trastuzumab concentration from initial trastuzumab concentration taken for the conjugation reaction.[30] The composition of each polymer is given in Table 1.

Table 1. Composition of synthesized polymers depending on attached targeting ligand

Polymer	Composition
Pentablock polymer	Native non-conjugated pentablock polymer
PentD	Doxorubicin-conjugated pentablock polymer (non-targeted)
PentD-FA	Folate targeted doxorubicin-conjugated pentablock polymer
PentD-Her	Trastuzumab targeted doxorubicin-conjugated pentablock polymer
PentD-FA-Her	Folate and trastuzumab (dual) targeted doxorubicin-conjugated pentablock polymer

Trastuzumab conjugation on the surface of nanoparticles was

further established by measuring zeta potential of NPs using DLS and by X-ray photoelectron spectroscopy (XPS). For XPS analysis, nanoparticle suspension was dried over a silicon substrate and elements on nanoparticle surface were identified by recording binding energy spectrum of sample from 0 to 1100 eV with pass energy of 80 eV in fixed transmission mode on XPS (SPECS, Germany).

Stability studies of nanoparticles

Nanoparticle stability was evaluated in water, normal saline (0.9% w/v NaCl) and DMEM media for 3 days. Briefly, 0.1 mL of 5 mg/mL nanoparticle suspension was mixed with 5 mL of respective medium at 37 ºC. Particle size of the nanoparticles was periodically determined by DLS.

Drug release studies

Known concentrations of NPs were dialyzed in phosphate buffer pH 7.4 and acetate buffer pH 5.0 at 120 rpm at 37 °C. Periodic sampling was carried out and samples were analyzed using UV-Visible spectrophotometer at 481 nm. Concentration of released doxorubicin was determined using doxorubicin standard calibration curve.

Hemolysis study and evaluation of endosomolytic behavior of pentablock polymer NPs

Hemocompatibility of NPs was evaluated by studying hemolysis behavior of NPs in PBS. Endosomolytic behavior of NPs was evaluated by studying hemolysis behavior of NPs in saline buffers of pH 6.2 (early endosomal pH) and pH 5.0 (endo-lysosomal pH) as reported previously.[31] Human blood samples were freshly collected in heparin tubes from healthy volunteers at IIT Delhi Hospital, New Delhi. Blood (2 mL) was centrifuged at 1500 rpm for 10 min to isolate RBCs. They were thoroughly washed three times with respective buffer and 50 µL of RBCs were diluted to 10 mL respective buffer to make RBC stock solution. Nanoparticle suspension (100 µL) in respective buffer was incubated with 100 µL RBC stock solution for 1 h at 37 °C at 120 rpm to have final concentration in the range 0.125-2 mg/mL. Samples were then centrifuged at 1500 rpm for 5 min and released hemoglobin from the supernatant was analyzed using UV-Visible spectrophotometer at 540 nm. Percent hemolysis was calculated relative to hemolysis caused by positive control (1% Triton X-100) and negative control (respective buffer) using following equation-

$$\text{Hemolysis (\%)} = \frac{(\text{Sample}_{540\text{nm}} - \text{Negative control}_{540\text{nm}})}{(\text{Positive control}_{540\text{nm}} - \text{Negative control}_{540\text{nm}})} \times 100$$

Coagulation studies

Nanoparticle suspension (100 µL) was incubated with 900 µL blood to give final concentration in the range 0.125-2 mg/mL at 37 °C for 1 h. Platelet poor plasma was obtained from blood by centrifugation at 4000 rpm for 10 min and incubated at 37 °C. For estimation of prothrombin time (PT), tissue factor was added to platelet poor plasma followed by excess calcium chloride solution (25 mM). For estimation of activated partial thromboplastin time (aPTT), micronized silica and cephalin were mixed with platelet poor plasma followed by calcium chloride solution (25 mM). PT and aPTT were determined based on fibrin clot formation time using automated coagulation analyzer (Diagnostica Stago, Germany).

Cell culture experiments

BT-474 cell line (breast cancer cells), MCF-7 (breast cancer cells) and L929 (mouse fibroblast cells) were obtained from NCCS, Pune, India. Cells were cultured in 25 cm^2 tissue culture flasks with Dulbecco's modified Eagle's medium (DMEM) supplemented with 10% fetal bovine serum and 1% penicillin-streptomycin solution in 5% CO_2 atmosphere at 37 ºC.

Cell viability studies

Effect of nanoparticles on viability of MCF-7 and L929 cells was analyzed using MTT cytotoxicity assay. Cells at a density of 1×10^4 cells/well were seeded in 96 well plates and incubated at 37 °C for 24 h in CO_2 incubator. Nanoparticle suspension (0.125-2 mg/mL) was incubated with the cells for 24 h. Then, media was replaced and cells were incubated with 10 µL of 5% MTT solution for 4 h. DMSO (200 µL) was further added in each well to dissolve formazan crystals and absorbance was measured on microplate spectrophotometer (PowerWave XS2, BioTek Instruments, USA) at 540 nm. Cell viability was calculated relative to positive control (1% Triton X-100) and negative control (PBS) using following equation-

$$\text{Cell viability (\%)} = \frac{(\text{Sample}_{540\text{nm}} - \text{Positive control}_{540\text{nm}})}{(\text{Negative control}_{540\text{nm}} - \text{Positive control}_{540\text{nm}})} \times 100$$

***In vitro* cellular uptake- qualitative assessment using confocal laser scanning microscopy (CLSM)**

Cellular uptake of nanoparticles in BT-474, MCF-7 and L929 cells was visualized using confocal laser scanning microscope. Cells were seeded in 6 well plates containing a cover slip at a density of 1×10^4 cells per well and incubated at 37 °C for 24 h in CO_2 incubator. Nanoparticles (concentration equivalent to 10 µg/mL doxorubicin) were incubated with cells at 37 °C for 4 h. Cells were then rinsed twice with PBS and fixed with 4% formaldehyde solution. After washing with PBS, cells were stained with 50 µL DAPI for 15 min and observed under CLSM (FluoView FV1000 Olympus, USA). Images were obtained at 100x magnification from fluorescence emitted by DAPI (460 nm) and doxorubicin (560 nm).

***In vitro* cellular uptake- quantitative assessment using flow cytometry**

To corroborate the CLSM study, flow cytometry was used for cellular uptake studies in BT-474, MCF-7 and L929 cells. Cells were seeded in 6-well plates at density of 1×10^5 cells/well and incubated for 24 h in CO_2 incubator. Cells were then incubated with nanoparticles (concentration equivalent to 10 µg/mL doxorubicin) at 37 °C for 4 h. Then cells were washed twice with PBS, trypsinized, and centrifuged at 3500 rpm (1127×g) for 5 min. Cell pellet was resuspended in 500 µL PBS in FACS tube and analyzed with blue laser in Flow Cytometer (BD FACS Aria III, USA) for cellular uptake of NPs. Data were analyzed using Flowing Software (Version 2.5.1, Turku Centre for Biotechnology, Finland).

Annexin V-FITC apoptosis assay

Cellular apoptosis in BT-474, MCF-7 and L929 cells induced by nanoparticles was evaluated using Annexin V-FITC apoptosis

assay. Cells at a density of 1×10^5 cells/well were seeded in 6-well plates and incubated at 37 °C for 24 h in CO_2 incubator. Cells were incubated with nanoparticles (concentration equivalent to 10 µg/mL doxorubicin) for 7 h at 37 °C. Cells were then washed twice with PBS, trypsinized and centrifuged at 3500 rpm (1127×g) for 5 min. Cell pellet was suspended in 100 µL Annexin V binding buffer in FACS tube followed by addition of Annexin V-FITC (5 µL) and propidium iodide (5 µL) and incubated for 20 min at room temperature in dark. Before FACS analysis, 400 µL of Annexin V binding buffer was added in FACS tube and cells were analyzed by Flow Cytometer. Data were analyzed using Flowing Software (Version 2.5.1, Turku Centre for Biotechnology, Finland).

Animal studies

Anticancer efficacy of nanosystem was evaluated using Ehrlich ascites tumor (EAT) bearing Swiss albino mice (25 ± 5 g; 8-9 weeks old). EAT cell line was received as a gift from Dr. B.S. Dwarakanath's lab, INMAS, New Delhi. All the experiments were conducted as per the guidelines of CPCSEA and the Animal Ethical Committee (796/IAEC/14) of AIIMS, New Delhi. Animals were housed in an animal house facility in polycarbonate cages with supply of chow food and purified water *ad libitum* under a controlled environment of 25 °C temperature and 12 h light/dark cycles.

***In vivo* antitumor efficacy**

Tumors were induced in mice by subcutaneous injection of 150 µL EAT cell suspension (~2×10^7 cells) on the dorsal side of mice. When tumor volumes reached about 200-250 mm^3, drug treatment was started with that day being designated as day 0. Animals were randomized into three groups with 6 animals in each group. Group I was Control *i.e.* PBS treated mice, group II consisted of free doxorubicin treated mice and group III consisted of PentD-FA-Her NPs treated mice. All formulations were given intravenously via tail vein at a dose, equivalent to 5 mg/kg doxorubicin, every third day for 15 days (*i.e.* day 0, 3, 6, 9, 12 and 15). Tumor dimensions were measured using Vernier caliper and tumor volume was calculated using following equation-

$$\text{Tumor volume} = 0.5 \times \text{length} \times \text{width}^2$$

Where, length represents the largest tumor diameter and width represents the perpendicular tumor diameter. On the last day of experiment (day 18), blood was collected from venous plexus of eyes of anesthetized mice followed by euthanization by cervical dislocation. Tumor and vital organs like heart, liver, kidneys, lungs and spleen were removed for histopathology studies.

Histopathological analysis of organs and tumor

Histopathological analysis of tumor and vital organs- heart, liver, kidneys, lungs and spleen were carried out to evaluate antitumor efficacy and toxicity of formulations in mice. Tumor and organs were collected from euthanized mice and were fixed in 10% buffered formalin solution at room temperature. Formalin fixed samples were embedded in paraffin blocks and were cut into 5 µm sections using a rotary microtome (Leica, Germany). The sections were then stained with hematoxyline and eosin (H&E) stains and were observed under light microscope.

Blood biochemistry analysis

Blood serum was analyzed for creatine kinase MB (CK-MB) using CK-MB Kit (Audit Diagnostics, Ireland) for cardiac damage assessment on Automated Analyzer (Cobas e411, Roche Diagnostics, USA). Serum was also tested for liver and kidney function tests for assessing hepatic and renal toxicity. All the measurements were carried out using Automated Biochemical Analyzer (TurboChem 100, Awareness Technology Inc., USA).

Statistical analysis

All *in vitro* data are expressed as mean ± standard deviation (SD), whereas *in vivo* data are expressed as mean ± standard error of mean (SEM). Statistical analysis was performed with Sigma Stat (Version 3.5, Systat Software Inc., San Jose, CA, USA) using one-way analysis of variance (one-way ANOVA) with Bonferroni multiple comparison test. The p-value < 0.05 was considered as statistically significant.

Results and discussion

Synthesis of PDMAEMA-PPEGMA-PCL-PPEGMA-PDMAEMA pentablock copolymer

Synthesis scheme of PDMAEMA-PPEGMA-PCL-PPEGMA-PDMAEMA pentablock copolymer is shown in Scheme 2. In the first step, hydroxyl groups of PCL diol were reacted with α-bromoisobutyryl bromide to synthesize PCL macroinitiator which was characterized using ^{1}H-NMR and ATR-FTIR (Supporting Information Fig. S1B and S2B, respectively). Presence of new peak at δ 1.95 ppm (peak i) in ^{1}H-NMR of PCL macroinitiator corresponds to geminal methyl groups of α-bromoisobutyryl bromide. Similarly, a peak corresponding to methylenic protons adjacent to hydroxyl groups in PCL diol (peak d) was shifted from δ 3.64 to δ 4.20 ppm due to carbonyl group of α-bromoisobutyryl bromide also established successful synthesis of PCL macroinitiator. According to FTIR spectrum (Supporting Information Fig. S2B), C-Br stretching vibration band at 642 cm^{-1} and absence of O-H stretching vibration band at 3430 cm^{-1} confirmed the synthesis of PCL macroinitiator.

PCL macroinitiator was then utilized for initiating atom transfer radical polymerization of PEGMA and DMAEMA in the presence of CuBr and PMDETA. Ratio of PEGMA/DMAEMA/Macroinitiator was kept at 10:5:1 to synthesize polymer with a molecular weight of ~6500 Da. Ratio of 1:1 was taken for CuBr/PMDETA to obtain higher activation rate constant in ATRP reaction. Synthesized polymer was analyzed using ^{1}H-NMR, ATR-FTIR and ^{13}C-NMR. In ^{1}H-NMR spectra (Supporting Information Fig. S1C), a peak at δ 3.66 ppm (peak e), corresponding to -OCH_2 groups from PEGMA chains and peak at δ 2.80 ppm (peak o) which corresponds to terminal N-methyl groups from DMAEMA, confirmed the synthesis of pentablock copolymer. It was calculated from the integration of ^{1}H-NMR peaks that 8 molecules of PEGMA and 4 molecules of DMAEMA were present in the pentablock copolymer with molecular weight of ~6000 Da, whereas GPC showed M_n and M_w of 6786 Da and 8006 Da respectively with polydispersity index of 1.179 (Supporting Information Fig. S3). ^{13}C-NMR spectra (Supporting Information Fig. S4) also confirmed the successful synthesis of pentablock copolymer. According to FTIR spectrum (Supporting Information Fig. S2C), O-H stretching vibration band in the region of 3400-3500 cm^{-1} and C-O-C vibration band at 1100 cm^{-1} confirmed the presence of PEGMA units in the pentablock copolymer. Similarly, C-N stretching

vibrations at 1239 cm^{-1} confirmed the attachment of DMAEMA units in the pentablock copolymer. Thus, polymer with desired molecular weight and uniform size distribution was synthesized using ATRP.

Conjugation of folic acid and doxorubicin with pentablock copolymer

Multiple PEG chains of pentablock copolymer were functionalized by reacting polymer with succinic anhydride followed by hydrazine to confer -$CONHNH_2$ functionality in the polymer in order to conjugate folic acid and doxorubicin to the pentablock copolymer. Formation of carboxylated pentablock copolymer (Pent-COOH) was confirmed using ^{1}H-NMR and ATR-FTIR (Supporting Information Fig. S1D and S2D, respectively). A peak at δ 2.75 (peak p), corresponding to -CH_2-CH_2 group of succinic acid confirmed the conjugation of succinic acid to the polymer with conversion of eight hydroxyl groups to eight -COOH groups in the PEG chains of the polymer. Also, broad O-H stretching vibration band of carboxyl group in the region 2600-3400 cm^{-1} in FTIR spectrum supports ^{1}H-NMR data.

Pent-COOH polymer was further reacted with hydrazine (six equivalents of -COOH groups) to synthesize Pent-$CONHNH_2$ polymer containing six -$CONHNH_2$ functionalities in the polymer chain. The synthesis of Pent-$CONHNH_2$ was confirmed by FTIR spectra (Supporting Information Fig. S2E) which showed the presence of a broad band at 3321 cm^{-1}, corresponding to aliphatic amines.

Folic acid was further conjugated with the pentablock copolymer by DCC-NHS mediated activation of γ-carboxylic acid of folic acid followed by reaction with -$CONHNH_2$ end groups of the polymer. Folate conjugated pentablock copolymer (Pent-FA) was characterized by ^{1}H-NMR, UV-Visible spectroscopy and CHN analysis. ^{1}H-NMR spectra (Supporting Information Fig. S1E) showed characteristic peaks of folic acid in the region δ6 - δ12, including aromatic proton shifts at δ6 - δ8 which corresponds to the aromatic region of folic acid, while retaining peaks from pentablock polymer, suggesting successful conjugation of folic acid with the polymer. UV-Visible spectroscopy (Supporting Information Fig. S5) also showed change in absorption spectrum of folic acid with blue shift in λ_{max} indicating successful conjugation of folic acid with the polymer. According to CHN analysis, C/N ratio of the Pent-FA polymer was found to be 10.94. Based on C/N ratio, it was found that ~2 molecules of folic acid have been conjugated to the single polymer chain.

Polymer was then conjugated with doxorubicin through hydrazone linkages by reacting carbonyl group of doxorubicin with -$CONHNH_2$ end groups of the polymer in DMSO for 24 h to obtain doxorubicin conjugated polymer (PentD and PentD-FA). Doxorubicin conjugation on the pentablock copolymer was characterized by UV-Visible spectroscopy and DSC. UV-Visible spectroscopy (Supporting Information Fig. S6) showed change in absorption spectrum of doxorubicin with red shift in λ_{max} indicating successful conjugation of doxorubicin with the polymer. Doxorubicin content of the polymer was found to be 175.36 µg/mg in PentD-FA polymer and 171.21 µg/mg in PentD polymer.

DSC studies for determination of doxorubicin conjugation with the polymer

Doxorubicin conjugation with the polymer was confirmed using DSC as shown in Fig. 1.

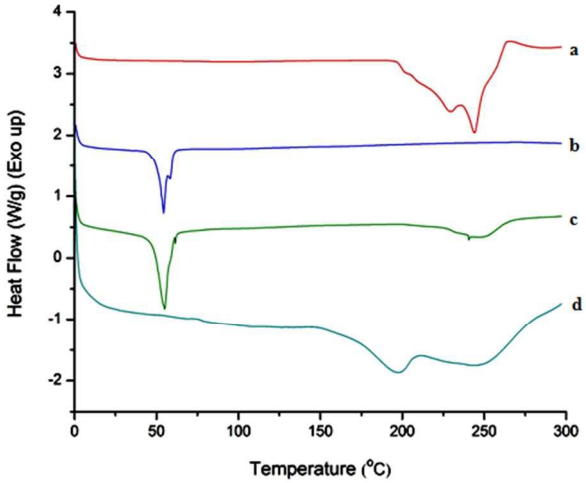

Fig. 1. DSC thermogram overlay of a) doxorubicin hydrochloride, b) pentablock copolymer, c) physical mixture of doxorubicin hydrochloride and pentablock copolymer and d) doxorubicin conjugated pentablock polymer, indicating successful doxorubicin conjugation with pentablock polymer.

DSC thermogram of pentablock polymer showed an endothermic peak at 54.32 °C which corresponds to melting peak of the polymer. Doxorubicin hydrochloride also showed two endothermic melting peaks at 228.95 °C and 243.86 °C. Characteristic endothermic peaks of pentablock copolymer and doxorubicin were observed in the physical mixture of pentablock copolymer and doxorubicin, whereas in doxorubicin conjugated polymer thermogram, the characteristic peaks of polymer and doxorubicin disappeared. Significant difference in thermal behavior of the doxorubicin-conjugated polymer was observed as compared to thermal behavior of pentablock copolymer or doxorubicin alone. This confirmed presence of strong covalent interactions between pentablock copolymer and doxorubicin molecules indicating successful chemical conjugation of doxorubicin with the polymer chains.

Preparation and characterization of nanoparticles

Nanoparticles were prepared by nanoprecipitation method developed by Fessi et al.[32] The nanoparticle size influences cellular uptake as well as systemic clearance of NPs and hence it is very important to prepare monodispersed nanoparticles with size ≤ 150 nm.

Polymeric nanoparticles prepared by nanoprecipitation showed narrow particle size distribution as indicated by low polydispersity index as shown in Table 2, indicating low batch to batch variation. The nanoparticle size increased slightly after trastuzumab conjugation while maintaining monodispersed nanoparticles.

Table 2. Nanoparticle characterization by DLS

Polymeric NPs	Particle size[a]	Polydispersity index[a]
PentD	112.5 ± 6.0 nm	0.083 ± 0.004
PentD-FA	122.3 ± 9.6 nm	0.093 ± 0.008
PentD-Her	137.0 ± 5.8 nm	0.138 ± 0.031
PentD-FA-Her	152.3 ± 3.3 nm	0.148 ± 0.029

[a] Mean ± SD, n=3

Nanoparticles were also characterized using AFM, SEM and TEM to determine absolute particle size of NPs as compared to hydrodynamic size obtained from DLS. AFM, SEM and TEM showed solid matrix structured nanoparticles with average size in the range 90-130 nm as shown in Fig. 2.

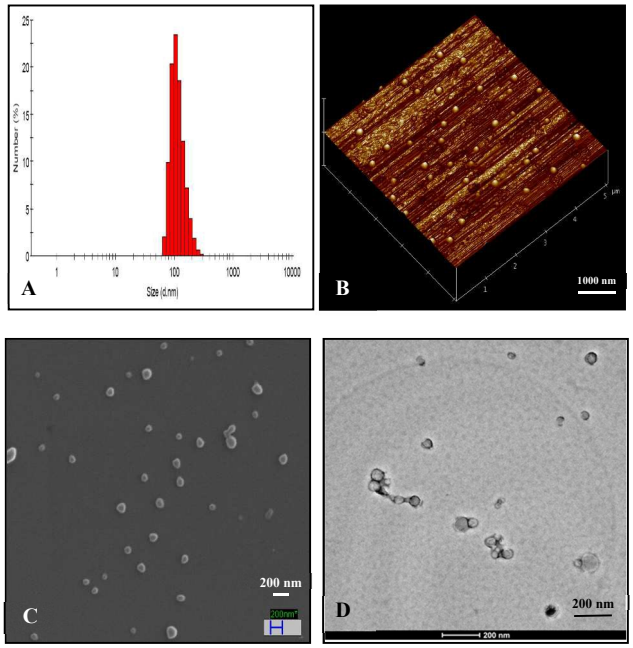

Fig. 2. PentD-FA-Her nanoparticle characterization studies using A) DLS, B) AFM, C) SEM and D) TEM showing polymeric nanoparticles with uniform particle size and narrow size distribution

Pluronic F-68 (1%) was used to prevent aggregation of nanoparticles during nanoprecipitation and easy redispersibility after lyophilization. To prevent nanoparticle aggregation during lyophilization and to improve the stability of nanoparticles during storage, trehalose was used as cryoprotectant at concentration of 10%. The reconstitution time of freeze dried nanoparticles was found to be ~1 min and nanoparticles were easily redispersible in water with uniform dispersion without any aggregation.

Trastuzumab conjugation

Trastuzumab was conjugated on nanoparticles using EDC-NHS chemistry. Carboxylic groups of polymeric nanoparticles were activated first and then reacted with amino groups of trastuzumab antibody to prepare trastuzumab conjugated NPs. Based on Biuret assay of filtrate containing unconjugated trastuzumab, concentration of trastuzumab conjugated on PentD-Her NPs and PentD-FA-Her NPs was determined to be 78.4 µg/mg and 75.9 µg/mg of nanoparticles, respectively.

Trastuzumab conjugation on nanoparticle surface was confirmed using zeta potential measurement and XPS. The zeta potential of PentD NPs and PentD-FA NPs before and after trastuzumab conjugation is shown in Table 3. The positive shift in zeta potential after trastuzumab conjugation can be attributed to positive charge of trastuzumab, which confirmed successful conjugation of trastuzumab on nanoparticle surface.

Table 3. Zeta potential measurement of nanoparticles for determination of trastuzumab conjugation[a]

Polymer	Zeta Potential (mV)	
	Before Conjugation	After Conjugation
PentD NPs	12.8 ± 0.2	18.8 ± 0.3
PentD-FA NPs	5.1 ± 0.1	13.8 ± 0.7

[a] Mean ± SD, n=3

Trastuzumab conjugation on nanoparticle surface was further confirmed by analyzing the surface chemistry of nanoparticles using XPS. Trastuzumab molecule consists of 1726 nitrogen atoms and hence gives stronger nitrogen N 1s signal in the binding energy range of 398-400 eV in XPS.[33] XPS wide scan spectra of unconjugated and conjugated polymer are shown in Fig. 3.

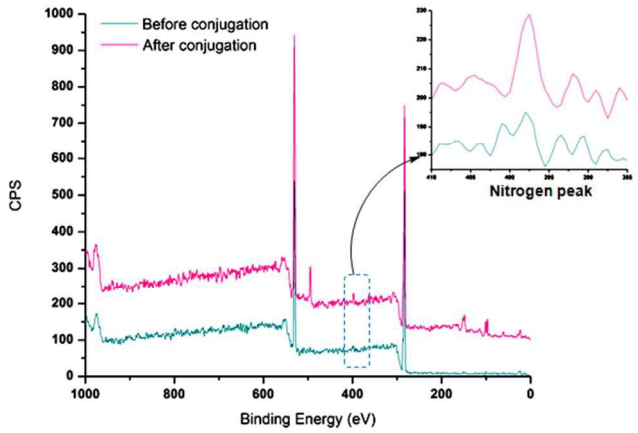

Fig. 3. XPS wide scan spectra of pentablock polymer before and after trastuzumab conjugation. Successful trastuzumab conjugation is evident from stronger nitrogen N 1s peak in the binding energy range of 398-400 eV in trastuzumab conjugated polymer.

In the XPS scan, unconjugated polymer showed very weak nitrogen signal (N 1s) at the binding energy of 398 eV, whereas after trastuzumab conjugation, nitrogen signal intensity was increased indicating increased nitrogen content of the NPs. This can be attributed to nitrogen from trastuzumab molecules. Thus, trastuzumab conjugation on nanoparticle surface was successfully characterized using zeta potential measurement and XPS.

Stability studies of nanoparticles

Stability is an essential parameter for nanoparticles intended for drug delivery applications. Nanoparticles can aggregate rendering them ineffective as drug delivery vehicles. These aggregates can cause clogging of blood vessels resulting in life threatening complications.[34] Hence stability of nanoparticles was determined in water, saline and DMEM media at 37 °C. No substantial change in nanoparticle size was observed in water, DMEM media and saline solution up to 72 h at 37 °C (Fig. 4). This indicates robust stability of the nanoparticles which assures longer circulation time and higher chances of tumor accumulation with

better therapeutic efficacy.

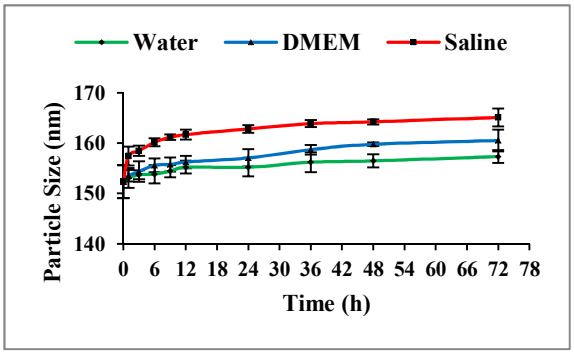

Fig. 4. Stability studies of PentD-FA-Her nanoparticles in water, saline and DMEM media showing robust stability. (Mean ± SD, n = 3)

Drug release studies

Drug release studies of doxorubicin conjugated polymeric nanoparticles was carried out in phosphate buffer pH 7.4 and in acetate buffer pH 5.0 which simulates extracellular pH and endo-lysosomal pH (pH 4.5-6.0), respectively. As shown in Fig. 5, doxorubicin release was found significantly higher in pH 5.0 as compared to pH 7.4. After 72 h, ~77% doxorubicin was released from the nanoparticles in pH 5.0 whereas only ~25% doxorubicin was released in pH 7.4. At the end of 7th day, ~89% doxorubicin was released in pH 5.0 as compared to ~29% release in pH 7.4. Higher doxorubicin release in acetate buffer pH 5.0 can be ascribed to acid responsive hydrazone bond between pentablock copolymer and doxorubicin. Acidic pH enhances breaking of hydrazone linkage resulting in faster and higher doxorubicin release from the nanoparticles. In acidic pH, nitrogen from hydrazone linkage (-C=**N**-NH$_2$) is protonated which increases the electrophilicity of carbon from hydrazone linkage (-**C**=N-NH$_2$). This causes increased susceptibility of hydrazone linkage to hydrolysis resulting in drug release.[35] Hence, at pH 5.0, doxorubicin release was faster as compared to that in pH 7.4. Thus, the acid responsive hydrazone bond prevents release of doxorubicin during the nanoparticle circulation in the blood and thus avoids toxicity to the normal cells that occurs in conventional doxorubicin chemotherapy.

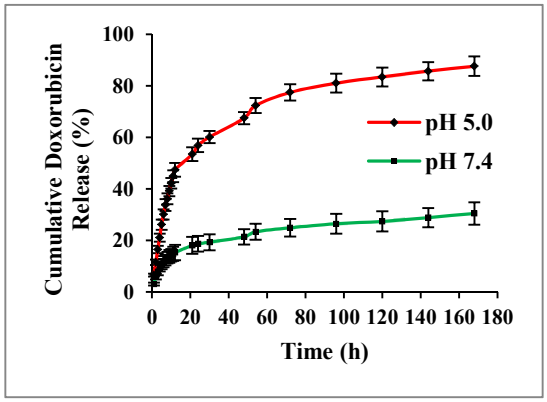

Fig. 5. Drug release studies of PentD-FA-Her nanoparticles in acetate buffer pH 5.0 and phosphate buffer pH 7.4 at 37 °C. (Mean ± SD, n = 3)

Hemolysis study

Hemocompatibility is an important criterion for safety and biocompatibility of nanoparticles intended as drug delivery carriers. Nanoparticles can interact with RBCs causing deformation of their cell membrane resulting in hemolysis. Hemoglobin released from the damaged RBCs can be determined spectrophotometrically at 540 nm. Hemoglobin absorbance is inversely proportional to the hemocompatibility of the nanoparticles. According to some researchers, less than 10% hemolysis is considered to be non-hemolytic while hemolysis greater than 25% is considered as hemolytic,[36, 37] whereas according to some studies, less than 20% hemolysis is considered to be hemocompatible.[38, 39] Interaction between RBCs and nanoparticles is considered to depend on surface charge as well as surface hydrophilicity of nanoparticles. Low surface charge and more hydrophilic surface prevent interaction of nanoparticles with RBCs resulting in low hemolysis.[40]

After incubating Pentablock polymer NPs with RBCs in PBS for 1 h at 37 °C, it was observed that nanoparticles at maximum concentration of 2.0 mg/mL caused ~11% hemolysis, whereas lower concentrations showed lower hemolysis as shown in Fig. 6. This can be attributed to low surface charge of nanoparticles and presence of multiple hydrophilic polyethylene glycol chains in the NPs. Thus, the results indicate the hemocompatibility of polymer nanoparticles in the concentration range 0.125 to 2.0 mg/mL.

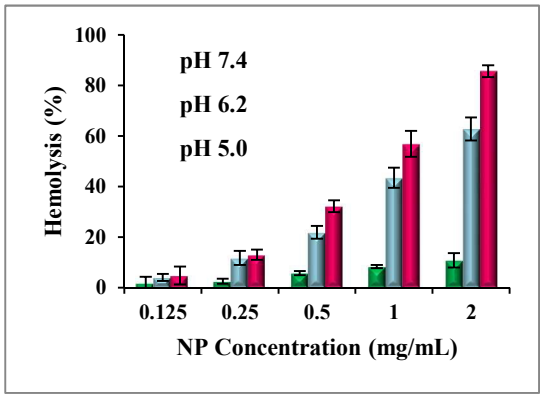

Fig. 6. Hemocompatibility and endosomolytic activity of Pentablock polymer NPs at pH 5.0, 6.2 and 7.4. (Mean ± SD, n = 3)

Endosomolytic behavior of NPs

pH dependent hemolysis assay is one of widely used techniques to determine the endosomolytic behavior/proton sponge effect of polymeric nanoparticles because RBC membrane mimics the lipid bi-layer membrane of endo-lysosomal vesicles. Hemolytic behavior in pH 7.4 determines hemocompatibility of polymer whereas hemolytic behavior in acidic media evaluates endosomolytic ability of the polymer.[31, 41-43]

After nanoparticle internalization in cancer cell, they are trafficked in the endo-lysosomal vesicles where due to low pH and various enzymes, drug can be degraded or it can be excreted out of the cell through exocytosis.[44] In order to prevent drug degradation and exocytosis, we designed our polymer with DMAEMA units in order to enhance endo-lysosomal escape of nanoparticles. At endo-lysosomal pH (pH ~4.5-6.0), DMAEMA units exhibit proton sponge effect through buffering action by binding protons present in the endo-lysosomes on tertiary nitrogen of DMAEM units. This results in increased influx of H$^+$

ions inside the endo-lysosomes to maintain H^+ ion concentration. This is followed by increased influx of Cl^- counterions inside the endosomes leading to rise in osmotic pressure. This leads to increased water influx causing vesicle swelling which subsequently leads to lysis of endo-lysosomes.[45]

In this experiment, RBCs were incubated with Pentablock polymer NPs in different pH saline buffers mimicking early endosomal pH (pH 6.2) and endo-lysosomal pH (pH 5.0). The amount of hemoglobin released in acidic pH is directly proportional to capacity of nanoparticles for endosomolytic behavior.

As shown in Fig. 6, nanoparticles exhibited higher hemolysis in acidic pH buffers as compared to that in pH 7.4. In early endosomal pH (pH 6.2) and in endo-lysosomal pH (pH 5.0), nanoparticles showed ~63% and ~86% hemolysis, respectively at 2 mg/mL concentration. Hemolysis was found to be dose-dependent with higher levels of hemolysis observed with increasing concentrations of NPs. Thus, polymeric nanoparticles exhibited endosomolytic activity and hence are useful in drug delivery applications for faster drug release from endo-lysosomes resulting in better therapeutic efficacy.

Coagulation studies

Nanoparticles can interact with platelets and other coagulation factors after intravenous administration causing activation of blood coagulation cascade. Nanoparticles can induce clotting inside blood vessels resulting in partial or complete blocking of blood vessels. Therefore, determination of thrombogenicity of nanoparticles is very essential for biocompatibility of nanoparticles.[46, 47]

Prothrombin time is associated with extrinsic coagulation pathway whereas activated partial thromboplastin time is associated with intrinsic coagulation pathway. Changes in any of these parameters are strong indicators of interaction of nanoparticles with the coagulation system. Pentablock polymer NPs were incubated with blood for 1 h for measurement of PT and aPTT. Healthy blood is reported to have PT values in the range 11-14 s, while for aPTT, range is 27-40 s.[48] As shown in Table 4, NPs in the concentration range 0.125 to 2 mg/mL did not show any apparent change in PT and aPTT. Both parameters were within normal range which indicated that nanoparticle did not interfere with coagulation pathway and did not cause activation of coagulation factors. Presence of multiple PEG chains on nanoparticle surface is expected to be responsible for biocompatibility of nanoparticles with respect to the coagulation system.

Table 4. Coagulation studies of Pentablock polymer NPs with respect to PT and aPTT [a]

NPs Concentration (mg/mL)	PT (s)	aPTT (s)
Control (PBS)	12.5 ± 0.2	30.3 ± 2.1
0.125	13.3 ± 0.9	31.3 ± 2.5
0.250	13.3 ± 0.9	32.7 ± 5.0
0.500	13.2 ± 1.3	32.7 ± 1.5
1.000	13.1 ± 0.8	34.7 ± 3.2
2.000	12.7 ± 1.4	32.0 ± 3.0

[a] Mean ± SD, n = 3

Cell culture studies

Cell lines were selected for this study based on receptor over-expression on the cell surface as shown in Table 5. BT-474 breast cancer cells overexpress HER2 receptors and also express folate RFα receptors. MCF-7 breast cancer cells overexpress folate RFα receptors and express few HER2 receptors. L929 is a non-cancerous mouse fibroblast cell line and is devoid of both HER2 and folate RFα receptors, thus acting as a control for the cellular uptake and apoptosis studies.

Table 5. Expression of RFα and HER2 receptors in cell lines [a]

Cell Line	RFα receptor	HER2 receptor	References
BT-474	+	+++	49, 50
MCF-7	+++	+	33, 51, 52
L929	-	-	53, 54

[a] +++: Over-expression, +: Medium to low expression, -: No expression

Cell viability studies

MTT assay was employed to determine cytotoxicity of polymeric NPs in MCF-7 and L929 cells. MTT assay measures cellular metabolic activity based on NADPH dependent dehydrogenase enzymes which reduce MTT dye to formazan crystals in viable cells. The formazan crystals give purple colored solution when dissolved in DMSO, which then can be quantified spectrophotometrically at 540 nm.[55]

In MCF-7 cells, Pentablock polymer NPs, in the concentration range 0.125 to 2 mg/mL, showed > 90% cell viability indicating biocompatible nature of the pentablock polymer. However, in case of doxorubicin conjugated polymeric NPs, viability of MCF-7 was slowly decreased with increase in NPs concentration from 0.125 to 2 mg/mL, with dual targeted NPs (PentD-FA-Her NPs) being more cytotoxic as compared to single targeted (PentD-FA and PentD-Her NPs) and non-targeted NPs (PentD NPs) as shown in Fig. 7. This can be attributed to folate and/or trastuzumab mediated enhanced cellular uptake of these NPs in MCF-7 cells resulting in higher cytotoxicity.

In case of L929 cell line, Pentablock polymer NPs showed cell viability above ~90% over the concentration range 0.125 to 2 mg/mL indicating their non-toxicity and biocompatibility towards normal (non-cancerous) cells. Doxorubicin conjugated polymeric NPs, irrespective of attached targeting ligand (PentD, PentD-FA, PentD-Her, PentD-FA-Her NPs), showed some cytotoxicity in concentration dependent manner as shown in Fig. 7. This can be assigned to non-specific cellular uptake of these NPs in L929 cells.

The results indicate the biocompatibility and non-toxicity of Pentablock polymer NPs in the concentration range 0.125 to 2 mg/mL and hence are appropriate as drug delivery carriers in cancer therapy.

Qualitative assessment of cellular uptake using CLSM

The cellular uptake of polymeric nanoparticles in BT-474, MCF-7 and L929 cell lines was evaluated using confocal laser scanning microscopy to determine cellular uptake efficiency of folate and/or trastuzumab functionalized polymeric NPs with respect to non-targeted NPs.

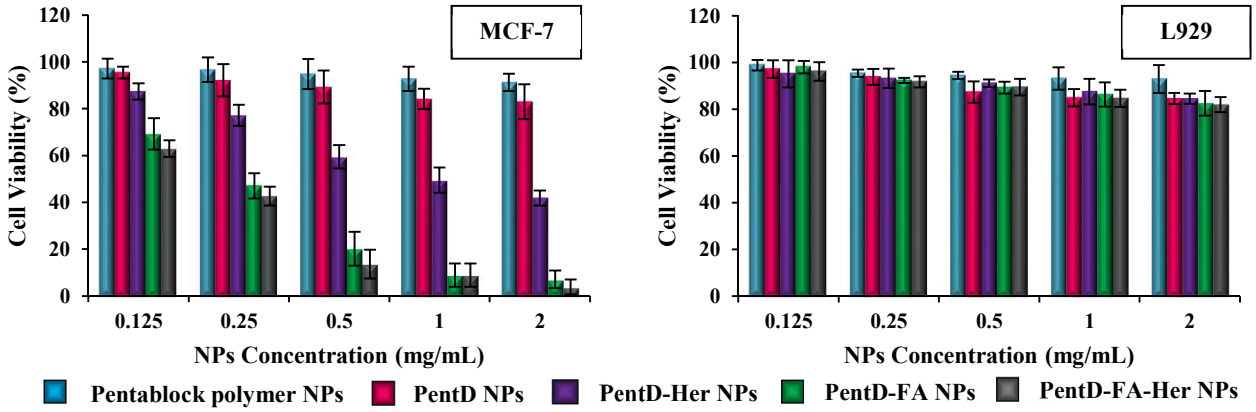

Fig. 7. MTT cytotoxicity assay of polymeric NPs with MCF-7 cells and L929 cells (mean ± SD, n = 3).

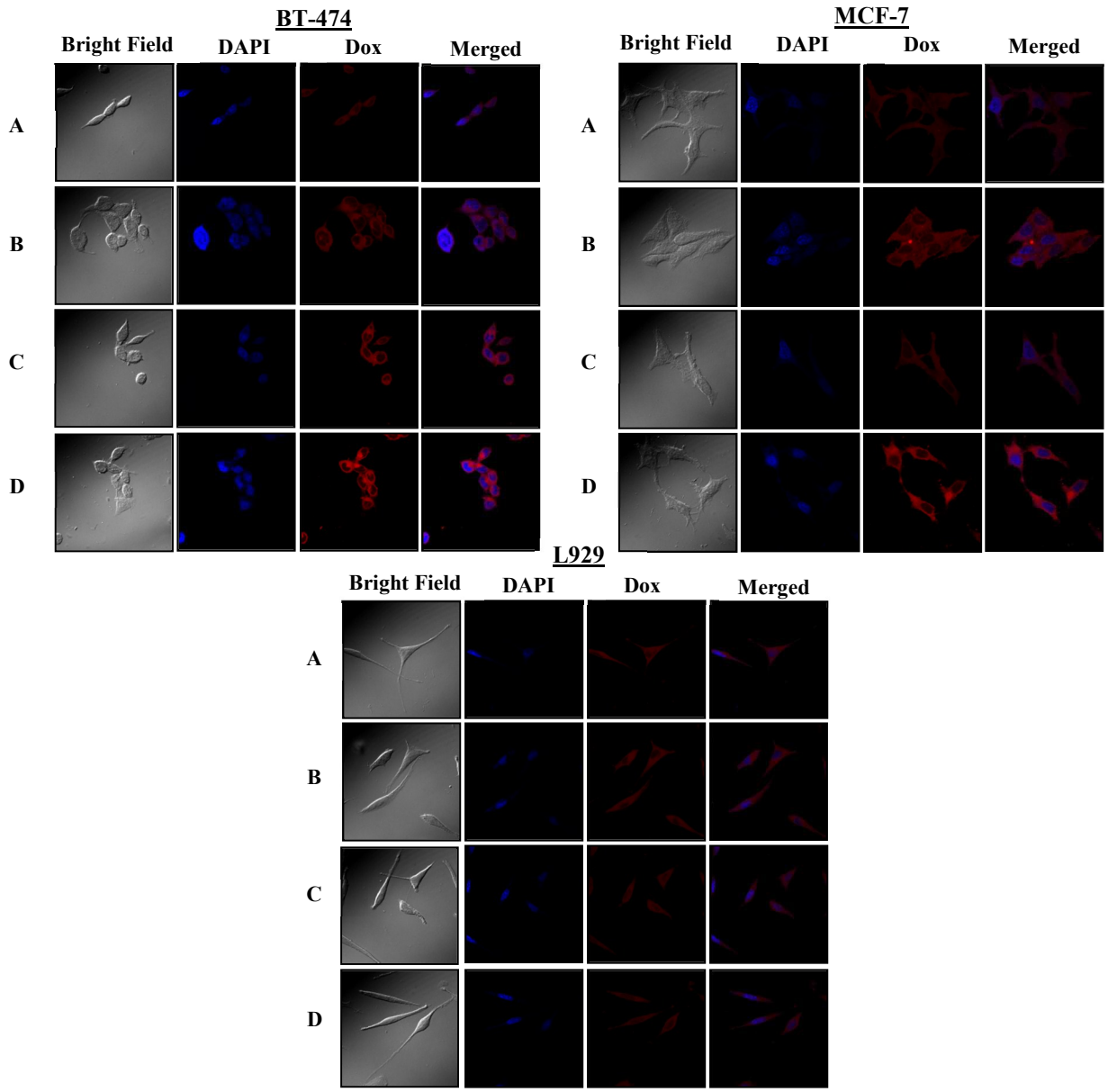

Fig. 8. Cellular uptake of NPs A) PentD NPs, B) PentD-FA NPs, C) PentD-Her NPs, and D) PentD-FA-Her NPs in BT-474, MCF-7 and L929 as observed by confocal laser scanning microscopy (100x magnification).

As shown in Fig. 8, in case of BT-474 and MCF-7 cell lines, cells treated with single targeted NPs (PentD-FA NPs and PentD-Her NPs) showed stronger doxorubicin fluorescence intensity as compared to non-targeted NPs (PentD NPs), indicating higher cellular uptake of single targeted NPs in the cancer cells. This can be attributed to folate RFα and HER2 receptor mediated endocytosis of NPs respectively. Dual targeted NPs (PentD-FA-Her NPs) showed even higher fluorescence intensity than single targeted NPs indicating higher cellular uptake of dual targeted NPs in BT-474 and MCF-7 cells. This higher cellular uptake is facilitated by folate RFα and HER2 receptor mediated endocytosis achieving higher doxorubicin concentration inside the cells. It also shows higher efficiency of dual targeted nanosystem for targeting and delivering doxorubicin to cancer cells.

L929 cells do not express either folate receptor RFα or HER2 receptor on their surface. As a result, significantly low doxorubicin fluorescence was observed in L929 cells irrespective of attached targeting ligand on NPs indicating some non-specific uptake of NPs by L929 cells as shown in Fig. 8.

Quantitative assessment of cellular uptake using flow cytometry

To validate and quantify the enhanced cellular uptake of dual targeted nanoparticles as observed in confocal microscopy studies, cellular uptake of NPs in BT-474, MCF-7 and L929 cell lines was analyzed using flow cytometry.

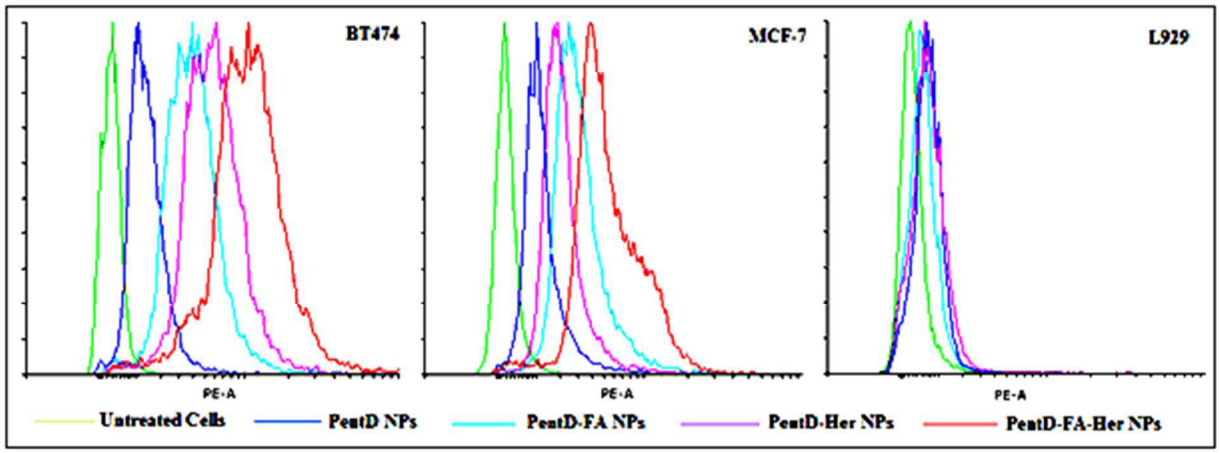

Fig. 9. Cellular uptake of nanoparticles in BT-474, MCF-7 and L929 cell lines as observed in flow cytometry

As shown in Fig. 9, in case of BT-474 cells, trastuzumab targeted NPs (PentD-Her NPs) showed ~4.5 and ~1.5 fold increase in median fluorescence intensity as compared to non-targeted NPs (PentD NPs) and folate targeted NPs (PentD-FA NPs) respectively. Since BT-474 over-expresses HER2 receptors, trastuzumab targeted NPs, having high affinity towards HER2 receptors, showed enhanced cellular uptake as compared to non-targeted as well as folate targeted NPs. Dual targeted NPs (PentD-FA-Her NPs) showed ~8.5 fold increase in median fluorescence intensity as compared to cells treated with non-targeted NPs and a ~2-3 fold increase in median fluorescence intensity compared to cells treated with single-targeted NPs (PentD-FA NPs and PentD-A NPs). Thus dual targeted NPs showed superior cellular uptake as compared to single and non-targeted NPs.

In case of MCF-7 cells, folate targeted NPs showed ~2.5 fold increase in median fluorescence intensity as compared to cells treated with non-targeted NPs (PentD NPs) and ~1.5 fold as compared to trastuzumab targeted NPs. This can be attributed to the fact that MCF-7 cell line over-expresses folate RFα receptors and expresses few HER2 receptors on its surface. Dual targeted NPs showed even higher median fluorescence intensity, ~1.7 fold and ~2.5 fold as compared to folate and trastuzumab targeted NPs respectively and ~4.5 fold as compared to non-targeted NPs, clearly indicating higher efficacy of dual targeting in cellular uptake of NPs in cancer cells.

In L929 cells, cells treated with all four types of NPs, irrespective of targeting moiety attached, showed low fluorescence intensity, indicating non-specific uptake of NPs which support the results of the confocal studies.

Thus, flow cytometry study supports confocal microscopy results about improved cellular uptake and higher cellular internalization of dual targeted NPs as compared to single and non-targeted NPs.

Annexin V-FITC apoptosis assay

Annexin V-FITC apoptosis assay is based on high binding affinity of Annexin V for exposed phosphatidylserine in apoptotic cells. Double staining with Annexin V-FITC and propidium iodide differentiates early apoptotic cells (AnnexinV-FITC^{+ve} PI^{-ve}) from viable cells (AnnexinV-FITC^{-ve} PI^{-ve}), and late apoptotic/necrotic cells (AnnexinV-FITC^{+ve} PI^{+ve}).[56]

As shown in Fig. 10, in case of BT-474 and MCF-7 cells, single targeted NPs (PentD-FA NPs and PentD-Her NPs) showed higher percent of early apoptotic cells as well as late apoptotic/necrotic cells as compared to non-targeted NPs (PentD NPs) due to receptor mediated cellular uptake of single targeted nanoparticles resulting in higher accumulation of doxorubicin in cancer cells. Dual-targeted NPs (PentD-FA-Her NPs) resulted in even higher percent of late apoptotic/necrotic cells as compared to single-targeted NPs, indicating its superior efficacy over single targeted NPs. In the case of L929 cells, majority of cells were found to be healthy and were negative for both Annexin V-FITC and propidium iodide (AnnexinV-FITC^{-ve} PI^{-ve}). All four NPs, irrespective of attached targeting moiety, showed similar results indicating low toxicity of the nanoparticles on normal cells which lack overexpressed folate RFα and HER2 receptors.

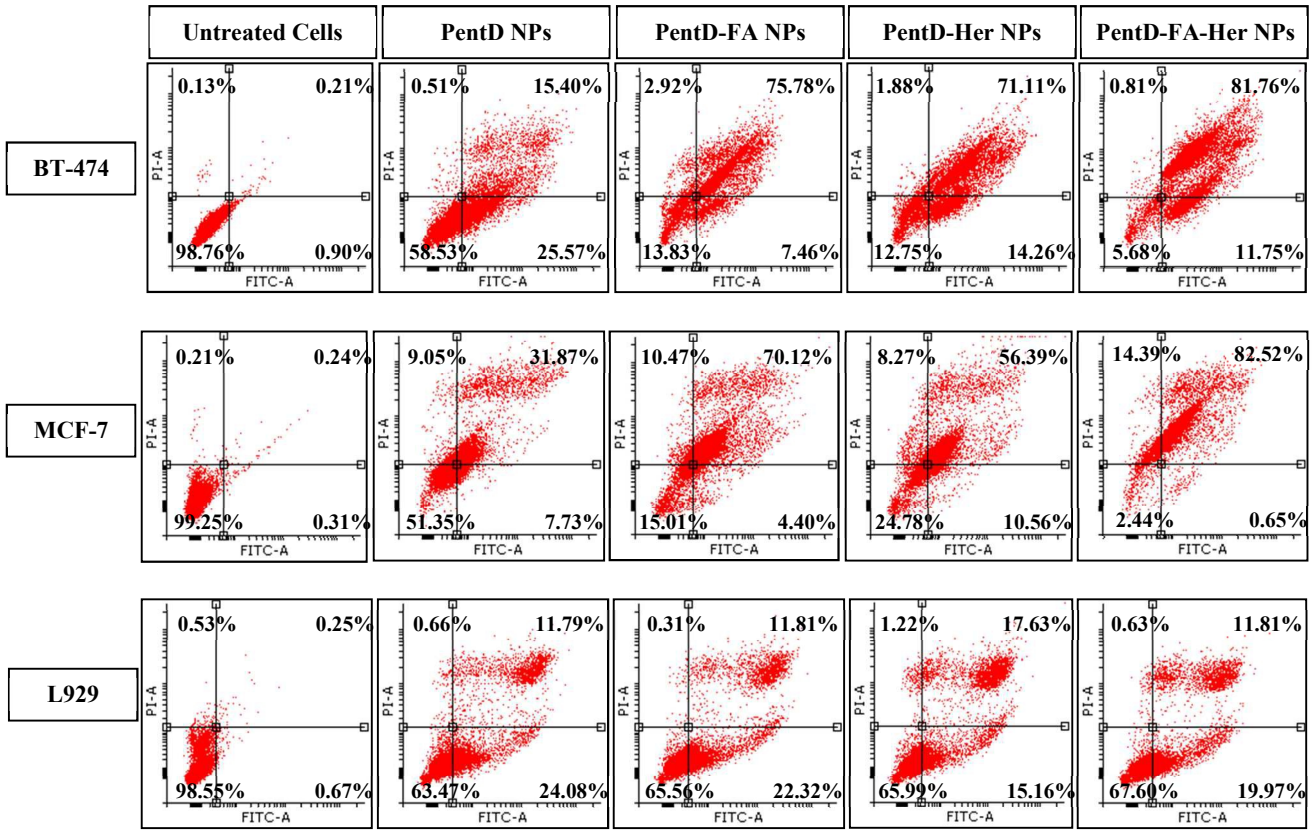

Fig. 10. Annexin V-FITC apoptosis assay for determining effect of nanoparticles on apoptosis/necrosis in BT-474, MCF-7, and L929 cells using flow cytometry

Significant increase in late apoptotic/necrotic cells observed in PentD-FA-Her NPs treated cancer cell lines BT-474 and MCF-7 can be attributed to enhanced cellular uptake of NPs leading to higher concentration of doxorubicin in cancer cells resulting in higher apoptosis. However, since L929 cells lack folate RFα receptor as well as HER2 receptor, these cells did not take up NPs resulting in lower apoptosis in L929 cell lines. Thus, we were able to selectively enhance apoptosis in cancer cells while protecting the non-cancerous cells from toxic effects of doxorubicin.

Animal studies

The Ehrlich ascites tumor (EAT) model is a transplantable tumor originated from mouse mammary carcinoma. It grows in ascitic as well as in solid forms. EAT cells are characterized by undifferentiated carcinoma, rapid proliferation rate and high transplantable capacity.[57] EAT cells significantly express folate RFα as well as HER2 receptors and hence the Ehrlich ascites tumor model was selected for evaluation of antitumor efficacy of PentD-FA-Her NPs.[58-60]

***In vivo* tumor regression study**

In vivo antitumor efficacy of PentD-FA-Her NPs and free doxorubicin was evaluated in Swiss albino mice bearing Ehrlich ascites tumor (EAT) model with PBS treated mice serving as Control.

As shown in Fig. 11, Control group consisting of PBS treated mice showed progressive increase in tumor size with increase in tumor volume up to 10 times on 18th day as compared to initial tumor volume on day 0. On 18th day, PentD-FA-Her NPs treated mice showed statistically significant superior antitumor efficacy as compared to Control ($p < 0.001$) as well as doxorubicin treated group ($p < 0.001$) with tumor volume reduction of ~92% as compared to initial tumor volume. Doxorubicin treated mice showed moderate antitumor efficacy with tumor volume reduction of ~38% as compared to initial tumor volume. The excellent antitumor efficacy of the PentD-FA-Her NPs can be attributed to higher accumulation in tumor due to dual targeting and by EPR effect, low protein adsorption leading to longer circulation half life, accelerated doxorubicin release from endosomes due to proton sponge effect and rapid endo-lysosomal release of doxorubicin due to pH responsive hydrazone linkage.

Determination of antitumor efficacy using histopathology

Antitumor efficacy of the nanosystem was further investigated using tumor histopathology as shown in Fig. 12. Tumor section of PBS treated mice showed viable neoplastic cells with very small necrosis area. In case of PentD-FA-Her NPs treated mice, tumor section showed tumor necrosis with very few viable neoplastic cells. Tumor section from free doxorubicin treated mice showed smaller necrosis area characterized by presence of necrotic cells as well as viable neoplastic cells. Thus, histology results corroborate with tumor regression study confirming enhanced antitumor efficacy of PentD-FA-Her NPs as compared to free doxorubicin treatment.

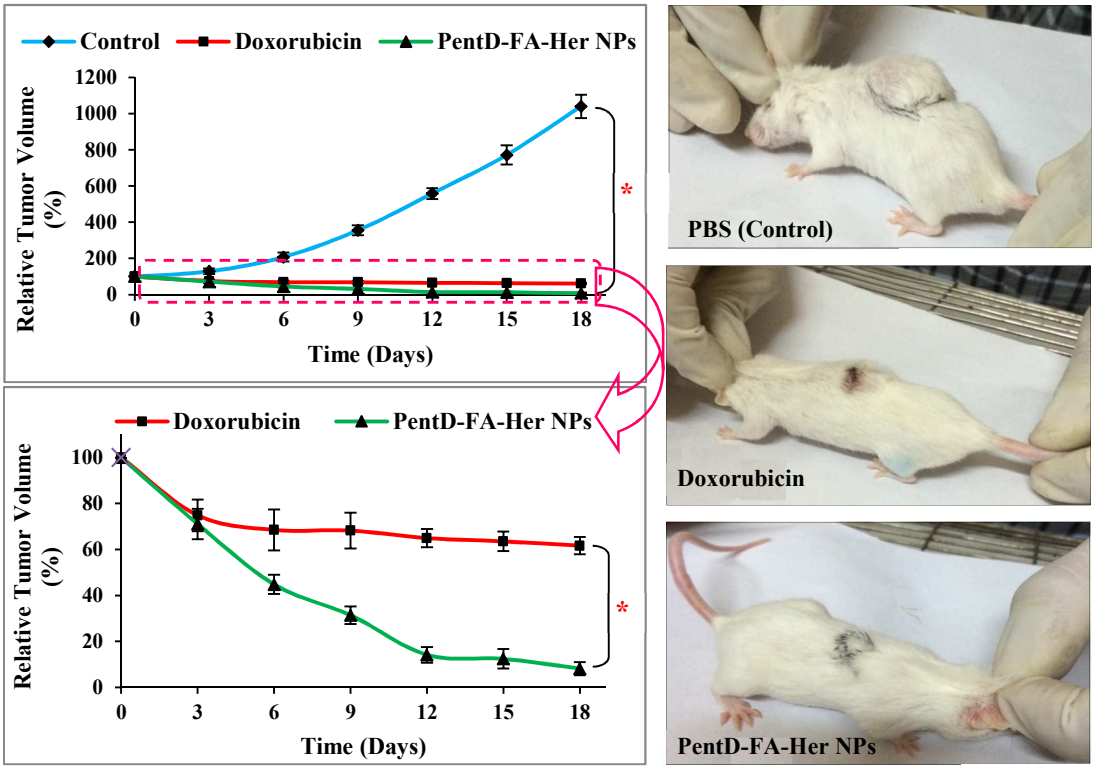

Fig. 11. *In vivo* tumor regression study of polymeric nanoparticles (PentD-FA-Her NPs) with respect to Control and free doxorubicin in Ehrlich ascites tumor (EAT) bearing Swiss albino mice. (mean ± SEM, n=6), $^{*}p < 0.001$. Tumor images of Ehrlich ascites tumor bearing Swiss albino mice treated with PBS (Control), free doxorubicin and polymeric nanoparticles (PentD-FA-Her NPs) as observed on 18th Day.

Organ toxicity studies based on histopathology

Doxorubicin is known to elicit cardiotoxicity and hence it is necessary to determine cardiac toxicity of nanoparticles loaded with doxorubicin to corroborate our hypothesis that nanoparticles will have lower cardiotoxicity as compared to doxorubicin alone due to its tumor targeted approach.

Cardiotoxicity of the formulations was investigated by histological analysis of heart from mice treated with free doxorubicin and PentD-FA-Her NPs as shown in Fig. 12. In case of free doxorubicin treated mice, heart tissue damage was evident with heart section showing disordered patterns of myofibrils, mild cardiomyocyte swelling, nuclear pyknosis and interstitial edema with significant cytoplasmic vacuolization suggesting cardiac tissue damage. However, heart section of nanoparticle treated mice showed very little disordered patterns of myofibrils with mild interstitial edema in the cardiac tissue and minimal cardiomyocyte swelling with occasional cytoplasmic vacuoles, indicating minimal cardiac damage and non-toxicity of nanoparticles to cardiac tissue. Thus, it can be inferred that cardiotoxicity of doxorubicin was overcome by PentD-FA-Her NPs while improving antitumor efficacy.

In vivo toxicity of PentD-FA-Her NPs was further investigated by histological analysis of other vital organs like liver, kidneys, lungs and spleen as shown in Fig. 12. Histology sections of liver from mice treated with free doxorubicin showed liver fibrosis manifested by presence of multiple focal cellular granulomatous lesions, foci of spotty necrosis and kupffer cell prominence. Free doxorubicin treatment also showed significant tubular damage and atrophy in the kidney. PentD-FA-Her NPs treatment, however, showed no difference in histology of these organs as compared to histology sections of Control indicating non-toxicity and biocompatibility of nanoparticles towards these vital organs.

The observed non-toxicity of PentD-FA-Her NPs can be attributed to polymer's low molecular weight and its biodegradable nature. It can also be attributed to PentD-FA-Her NPs active targeting of cancer cells via folate and trastuzumab ligands and passive targeting via EPR effect, which caused higher accumulation in tumor as compared to other tissues/organs leading to apparent non-toxicity. Also, since doxorubicin was covalently conjugated to the polymer via pH responsive hydrazone linkage, doxorubicin leakage/release during nanoparticle circulation was prevented leading to improved biocompatibility and minimal side effects. Thus, the developed nanosystem showed high biocompatibility with improved therapeutic index as compared to free doxorubicin therapy.

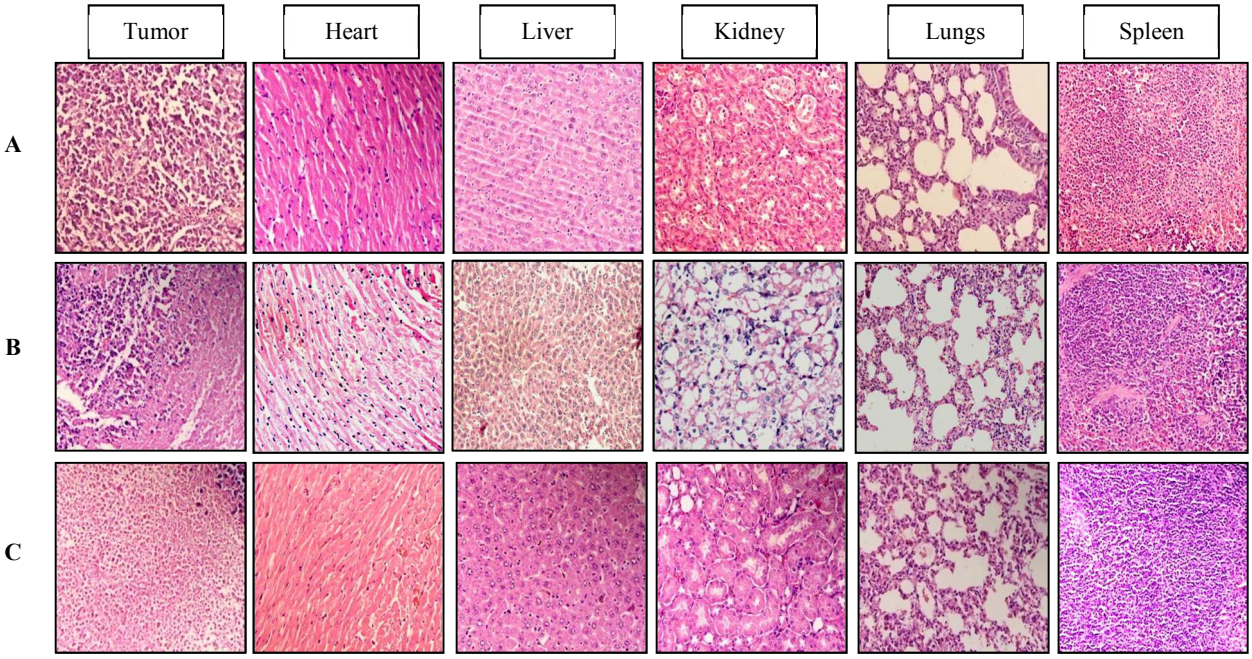

Fig. 12. Histological analysis of tumor and vital organs- heart, liver, kidney, lungs and spleen after chemotherapeutic treatment of PentD-FA-Her NPs and free doxorubicin in Ehrlich ascites tumor bearing Swiss albino mice. A) PBS treatment (Control), B) Doxorubicin treatment, C) PentD-FA-Her NPs treatment. Tissue sections were stained using H&E staining and observed under microscope at 20x magnification.

Serum biochemistry analysis

In vivo toxicity of the formulations was further investigated by serum biochemistry analysis as shown in Table 6.

Table 6. Serum biochemical analysis of Ehrlich ascites tumor bearing Swiss albino mice treated with PentD-FA-Her NPs and free doxorubicin[a]

Biochemical Parameter	Control (PBS)	Doxorubicin	PentD-FA-Her NPs
CK-MB (IU/L)	2.00 ± 0.58	11.67 ± 1.45*	4.00 ± 0.58
AST (SGOT) (IU/L)	55.97 ± 1.91	103.60 ± 3.04*	61.33 ± 1.74
ALT (SGPT) (IU/L)	31.53 ± 1.87	72.83 ± 3.13**	37.67 ± 1.87
Alkaline Phosphatase (IU/L)	112.97 ± 1.99	196.77 ± 5.04*	124.03 ± 2.96
Total Bilirubin (mg/dL)	0.24 ± 0.02	0.54 ± 0.05**	0.31 ± 0.03
Total Protein (mg/dL)	6.13 ± 0.18	5.67 ± 0.29	6.13 ± 0.15
Albumin (mg/dL)	3.47 ± 0.20	3.13 ± 0.15	3.30 ± 0.12
Globulin (mg/dL)	1.73 ± 0.12	1.50 ± 0.06	1.77 ± 0.12
A:G Ratio	2.04 ± 0.26	2.09 ± 0.02	1.88 ± 0.06
Total Cholesterol (mg/dL)	113.10 ± 2.87	120.17 ± 1.86	118.17 ± 1.30
Urea (mg/dL)	34.47 ± 2.45	69.93 ± 1.63*	40.33 ± 0.78
Creatinine (mg/dL)	0.30 ± 0.02	0.63 ± 0.03*	0.39 ± 0.02
Uric Acid (mg/dL)	2.57 ± 0.18	6.10 ± 0.21*	2.33 ± 0.15
Calcium (mg/dL)	7.90 ± 0.23	7.30 ± 0.21	7.40 ± 0.21
Phosphorus (mg/dL)	2.93 ± 0.15	3.40 ± 1.45	2.63 ± 0.24

[a] All values are expressed as mean ± SEM (n=3). *Highly significant ($p < 0.001$); **Significant ($p < 0.05$)

To determine cardiac toxicity of PentD-FA-Her NPs, cardiac specific biomarker- creatine kinase MB (CK-MB) was analyzed for cardiac damage. Creatine kinase MB, a specific and selective cardiac biomarker, is released in the blood after cardiac tissue damage and hence is wildly used to determine cardiac damage/toxicity.[61] Free doxorubicin treated mice showed significantly high levels of CK-MB in serum as compared to Control ($p < 0.001$) indicating cardiac damage/cardiotoxicity. Serum samples of mice treated with PentD-FA-Her NPs showed no significant variation in CK-MB levels as compared to PBS group ($p > 0.05$) indicating cardiac biocompatibility of PentD-FA-Her NPs.

Liver damage/hepatotoxicity was evaluated using liver biomarkers- aspartate transaminases (AST/SGOT), alanine transaminases (ALT/SGPT), alkaline phosphatase (ALP) and total bilirubin in the blood. Serum AST and ALP levels in free doxorubicin treated mice were significantly higher as compared to Control ($p < 0.001$). Free doxorubicin treated mice also showed higher serum ALT and total bilirubin levels as compared to Control ($p < 0.05$). In case of PentD-FA-Her NPs treated mice, there was statistically insignificant elevation in serum AST, ALT, ALP and total bilirubin levels ($p > 0.05$) compared to Control indicating non-toxicity of nanoparticles with respect to liver. Free doxorubicin also showed nephrotoxicity with significant elevation in blood urea, creatinine and uric acid levels as compared to Control ($p < 0.001$), whereas PentD-FA-Her NPs treated mice showed insignificant elevation in these parameters when compared to PBS group ($p > 0.05$) indicating non-toxicity to kidney.

Thus, based on serum biochemistry analysis, PentD-FA-Her NPs did not cause cardiotoxicity, hepatotoxicity and nephrotoxicity at therapeutic dose exhibited by free doxorubicin. This can be attributed to low drug release at physiological pH due to acid sensitive hydrazone linkage between doxorubicin and the polymer. Thus, we were able to reduce the toxicities associated with doxorubicin (cardiotoxicity, hepatotoxicity and

nephrotoxicity) using multifunctional nanoparticles with enhanced chemotherapeutic antitumor efficacy.

Conclusions

The present study investigated the combined activity of pH sensitivity and proton sponge effect for improved doxorubicin delivery from multifunctional polymeric nanosystem in breast cancer. ATRP based PDMAEMA-PPEGMA-PCL-PPEGMA-PDMAEMA pentablock copolymer was successfully synthesized with narrow molecular weight distribution. Polymeric nanoparticles showed uniform particle size in the range of ~150 nm with low polydispersity. Pentablock polymer was found to be biocompatible with respect to hemolysis, coagulation and MTT assay. Dual targeting (folate and trastuzumab), hydrazone linkage and endo-lysosomal escape ability resulted in superior therapeutic efficacy of multifunctional nanoparticles in *in vivo* studies with achieving significantly higher rate of tumor regression as compared to free doxorubicin with minimal cardiotoxicity, hepatotoxicity and nephrotoxicity associated with free doxorubicin chemotherapy. Thus, the multifunctional polymeric nanosystem exhibits potential as a promising drug delivery nanocarrier in breast cancer therapy and shows promise to be able to translate to clinical applications.

Acknowledgements

Shantanu V. Lale is thankful to Department of Biotechnology (DBT), India for the funding grant (BT/PR13341/NNT/28/467/2009). He extends his gratitude to the Indian Institute of Technology, Delhi for awarding him an Institute Fellowship. He is thankful to Prof. Renu Saxena and Dr. Archana Bansal from All India Institute of Medical Sciences (AIIMS), New Delhi for their help with the coagulation studies and CK-MB determination, respectively. He is thankful to Dr. Shyam B. Prasad for his help with flow cytometry. He is also thankful to Dr. Nadeem Tanveer from University College of Medical Sciences, Delhi for his help with the histopathology analysis.

Notes and references

[a] *Centre for Biomedical Engineering, Indian Institute of Technology Delhi, New Delhi 110016, India*
Tel: +91 11 26591041
Email: veenak_iitd@yahoo.com
[b] *Biomedical Engineering Unit, All India Institute of Medical Sciences, New Delhi 110029, India*
[c] *Department of Pathology, All India Institute of Medical Sciences, New Delhi 110029, India*
[d] *Division of Molecular Oncology, Institute of Cytology and Preventive Oncology, Noida 201301, India*

† Electronic Supplementary Information (ESI) available: [Polymer characterization data - ^{1}H-NMR, ^{13}C-NMR, FTIR, GPC and UV-Visible spectroscopy is provided in the Electronic Supplementary Information]. See DOI: 10.1039/b000000x/

1. S. Lv, M. Li, Z. Tang, W. Song, H. Sun, H. Liu and X. Chen, *Acta Biomater.*, 2013, **9**, 9330-9342.
2. N. Dube, J. Y. Shu, H. Dong, J. W. Seo, E. Ingham, A. Kheirolomoom, P. Y. Chen, J. Forsayeth, K. Bankiewicz, K. W. Ferrara and T. Xu, *Biomacromolecules*, 2013, **14**, 3697-3705.
3. R. Misra, M. Das, B. S. Sahoo and S. K. Sahoo, *Int. J. Pharm.*, 2014, **475**, 372-384.
4. I. Brigger, C. Dubernet and P. Couvreur, *Adv. Drug Delivery Rev.*, 2012, **64,** Supplement, 24-36.
5. X. Hu, R. Wang, J. Yue, S. Liu, Z. Xie and X. Jing, *J. Mater. Chem.*, 2012, **22**, 13303-13310.
6. Y. Zhong, F. Meng, C. Deng and Z. Zhong, *Biomacromolecules*, 2014, **15**, 1955-1969.
7. T. Etrych, V. Subr, R. Laga, B. Rihova and K. Ulbrich, *Eur. J. Pharm. Sci.*, 2014, **58**, 1-12.
8. C. Zhang, D. Pan, K. Luo, N. Li, C. Guo, X. Zheng and Z. Gu, *Polym. Chem.*, 2014, **5**, 5227-5235.
9. Y. Du, W. Chen, M. Zheng, F. Meng and Z. Zhong, *Biomaterials*, 2012, **33**, 7291-7299.
10. S. J. Lee, K. H. Min, H. J. Lee, A. N. Koo, H. P. Rim, B. J. Jeon, S. Y. Jeong, J. S. Heo and S. C. Lee, *Biomacromolecules*, 2011, **12**, 1224-1233.
11. T. Jiang, Y. M. Li, Y. Lv, Y. J. Cheng, F. He and R. X. Zhuo, *Colloids Surf., B*, 2013, **111**, 542-548.
12. K. Wang, X. Zhang, Y. Liu, C. Liu, B. Jiang and Y. Jiang, *Biomaterials*, 2014, **35**, 8735-8747.
13. J. Liu, Y. Huang, A. Kumar, A. Tan, S. Jin, A. Mozhi and X.-J. Liang, *Biotechnol. Adv.*, 2014, **32**, 693-710.
14. S. V. Lale, R. G. Aswathy, A. Aravind, D. S. Kumar and V. Koul, *Biomacromolecules*, 2014, **15**, 1737-1752.
15. K. Greish, T. Sawa, J. Fang, T. Akaike and H. Maeda, *J. Controlled Release*, 2004, **97**, 219-230.
16. L. Li, Q. Yang, Z. Zhou, J. Zhong and Y. Huang, *Biomaterials*, 2014, **35**, 5171-5187.
17. T. Etrych, V. Subr, J. Strohalm, M. Sirova, B. Rihova and K. Ulbrich, *J. Controlled Release*, 2012, **164**, 346-354.
18. M. A. Woodruff and D. W. Hutmacher, *Prog. Polym. Sci.*, 2010, **35**, 1217-1256.
19. W. B. Liechty, D. R. Kryscio, B. V. Slaughter and N. A. Peppas, *Annu. Rev. Chem. Biomol. Eng.*, 2010, **1**, 149-173.
20. L. Chang, J. Liu, J. Zhang, L. Deng and A. Dong, *Polym. Chem.*, 2013, **4**, 1430-1438.
21. C. Gong, Z. Qian, C. Liu, M. Huang, Y. Gu, Y. Wen, B. Kan, K. Wang, M. Dai, X. Li, M. Gou, M. Tu and Y. Wei, *Smart Mater. Struct.*, 2007, **16**, 927-933.
22. K. Matyjaszewski and N. V. Tsarevsky, *J. Am. Chem. Soc.*, 2014, **136**, 6513-6533.
23. S. Yu, R. Dong, J. Chen, F. Chen, W. Jiang, Y. Zhou, X. Zhu and D. Yan, *Biomacromolecules*, 2014, **15**, 1828-1836.
24. S. Veeranarayanan, A. C. Poulose, M. S. Mohamed, S. H. Varghese, Y. Nagaoka, Y. Yoshida, T. Maekawa and D. S. Kumar, *Small*, 2012, **8**, 3476-3489.
25. D. D. Lane, D. Y. Chiu, F. Y. Su, S. Srinivasan, H. B. Kern, O. W. Press, P. S. Stayton and A. J. Convertine, *Polym. Chem.*, 2015, DOI: 10.1039/c1034py01250j.
26. H. L. Chu, H. W. Chen, S. H. Tseng, M. H. Hsu, L. P. Ho, F. H. Chou, M. P. Li, Y. C. Chang, P. H. Chen, L. Y. Tsai, C. C. Chou, J.

S. Chen, T. M. Cheng and C. C. Chang, *ChemMedChem*, 2014, **9**, 1023-1029.
27. Y. Tao, J. He, M. Zhang, Y. Hao, J. Liu and P. Ni, *Polym. Chem.*, 2014, **5**, 3443-3452.
28. L. E. Kelemen, *Int. J. Cancer*, 2006, **119**, 243-250.
29. J. Baselga, *Ann. Oncol.*, 2001, **12**, S49-55.
30. J. Zhao and S. S. Feng, *Biomaterials*, 2014, **35**, 3340-3347.
31. B. C. Evans, C. E. Nelson, S. S. Yu, K. R. Beavers, A. J. Kim, H. Li, H. M. Nelson, T. D. Giorgio and C. L. Duvall, *J. Vis. Exp.*, 2013, e50166.
32. H. Fessi, F. Puisieux, J. P. Devissaguet, N. Ammoury and S. Benita, *Int. J. Pharm.*, 1989, **55**, R1-R4.
33. Y. Liu, K. Li, B. Liu and S. S. Feng, *Biomaterials*, 2010, **31**, 9145-9155.
34. C. Song, J. Wu, C. Jiang, X. Shen, Q. Qiao and Y. Hu, *Mol. Pharmaceutics*, 2013, **10**, 3555-3563.
35. J. Kalia and R. T. Raines, *Angew. Chem. Int. Ed.*, 2008, **47**, 7523-7526.
36. M. A. Dobrovolskaia, J. D. Clogston, B. W. Neun, J. B. Hall, A. K. Patri and S. E. McNeil, *Nano Lett.*, 2008, **8**, 2180-2187.
37. K. Amin and R. M. Dannenfelser, *J. Pharm. Sci.*, 2006, **95**, 1173-1176.
38. J. F. Krzyzaniak, F. A. Alvarez-Nunez, D. M. Raymond and S. H. Yalkowsky, *J. Pharm. Sci.*, 1997, **86**, 1215-1217.
39. F. L. Fort, I. A. Heyman and J. W. Kesterson, *J. Parenter. Sci. Technol.*, 1984, **38**, 82-87.
40. K. K. Upadhyay, A. K. Mishra, K. Chuttani, A. Kaul, C. Schatz, J. F. Le Meins, A. Misra and S. Lecommandoux, *Nanomed. Nanotechnol. Biol. Med.*, 2012, **8**, 71-80.
41. S. M. Henry, M. E. El-Sayed, C. M. Pirie, A. S. Hoffman and P. S. Stayton, *Biomacromolecules*, 2006, **7**, 2407-2414.
42. V. Bulmus, M. Woodward, L. Lin, N. Murthy, P. Stayton and A. Hoffman, *J. Controlled Release*, 2003, **93**, 105-120.
43. N. Murthy, J. Campbell, N. Fausto, A. S. Hoffman and P. S. Stayton, *Bioconjugate Chem.*, 2003, **14**, 412-419.
44. Y. Wang, Y. Liu, Y. Liu, Y. Wang, J. Wu, R. Li, J. Yang and N. Zhang, *Polym. Chem.*, 2014, **5**, 423-432.
45. K. Seo and D. Kim, *Acta Biomater.*, 2010, **6**, 2157-2164.
46. A. N. Ilinskaya and M. A. Dobrovolskaia, *Nanomedicine (Lond.)*, 2013, **8**, 969-981.
47. L. C. Xu, J. W. Bauer and C. A. Siedlecki, *Colloids Surf., B*, 2014, **124**, 49-68.
48. S. A. Santoro and C. S. Eby, in *Hematology: Basic principles and practice*, eds. Hoffman R, Benz EJ and S. J. Shattil, Churchill Livingstone Elsevier, Philadelphia, 2000, pp. 1841-1850.
49. K. Subik, J. F. Lee, L. Baxter, T. Strzepek, D. Costello, P. Crowley, L. Xing, M. C. Hung, T. Bonfiglio, D. G. Hicks and P. Tang, *Breast Cancer (Auckl)*, 2010, **4**, 35-41.
50. R. M. Neve, K. Chin, J. Fridlyand, J. Yeh, F. L. Baehner, T. Fevr, L. Clark, N. Bayani, J. P. Coppe, F. Tong, T. Speed, P. T. Spellman, S. DeVries, A. Lapuk, N. J. Wang, W. L. Kuo, J. L. Stilwell, D. Pinkel, D. G. Albertson, F. M. Waldman, F. McCormick, R. B. Dickson, M. D. Johnson, M. Lippman, S. Ethier, A. Gazdar and J. W. Gray, *Cancer Cell*, 2006, **10**, 515-527.
51. M. V. Yezhelyev, A. Al Hajj, C. Morris, A. I. Marcus, T. Liu, M. Lewis, C. Cohen, P. Zrazhevskiy, J. W. Simons, A. Rogatko, S. Nie, X. Gao and R. M. O'Regan, *Adv. Mater.*, 2007, **19**, 3146-3151.
52. R. Nahire, M. K. Haldar, S. Paul, A. Mergoum, A. H. Ambre, K. S. Katti, K. N. Gange, D. K. Srivastava, K. Sarkar and S. Mallik, *Biomacromolecules*, 2013, **14**, 841-853.
53. D. Bhattacharya, M. Das, D. Mishra, I. Banerjee, S. K. Sahu, T. K. Maiti and P. Pramanik, *Nanoscale*, 2011, **3**, 1653-1662.
54. H. Zolata, F. A. Davani and H. Afarideh, *Nucl. Med. Biol.*, 2014, DOI:10.1016/j.nucmedbio.2014.1009.1007.
55. M. Butler and M. Spearman, in *Animal cell biotechnology: Methods and protocols*, ed. R. Portner, Humana Press, New Jersey, 2007, pp. 205-222.
56. Hingorani R, Deng J, Elia J, McIntyre C and D. Mittar, https://www.bdbiosciences.com/documents/BD_FACSVerse_Apoptosis_Detection_AppNote.pdf assessed on December 2014.
57. Ozaslan M, Karagoz ID, Kilic IH and M. Guldur, *Afr. J. Biotechnol.*, 2011, **10**, 2375-2378.
58. A. Elexpuru, M. Soriano and A. Villalobo, *Biol. Chem. H-S*, 1994, **375**, 293-298.
59. D. C. Soares, M. C. de Oliveira, A. L. de Barros, V. N. Cardoso and G. A. Ramaldes, *Eur. J. Pharm. Sci.*, 2011, **43**, 290-296.
60. N. Parker, M. J. Turk, E. Westrick, J. D. Lewis, P. S. Low and C. P. Leamon, *Anal. Biochem.*, 2005, **338**, 284-293.
61. D. J. Robinson and R. H. Christenson, *J. Emerg. Med.*, 1999, **17**, 95-104.

Table of Contents- Graphical Abstract

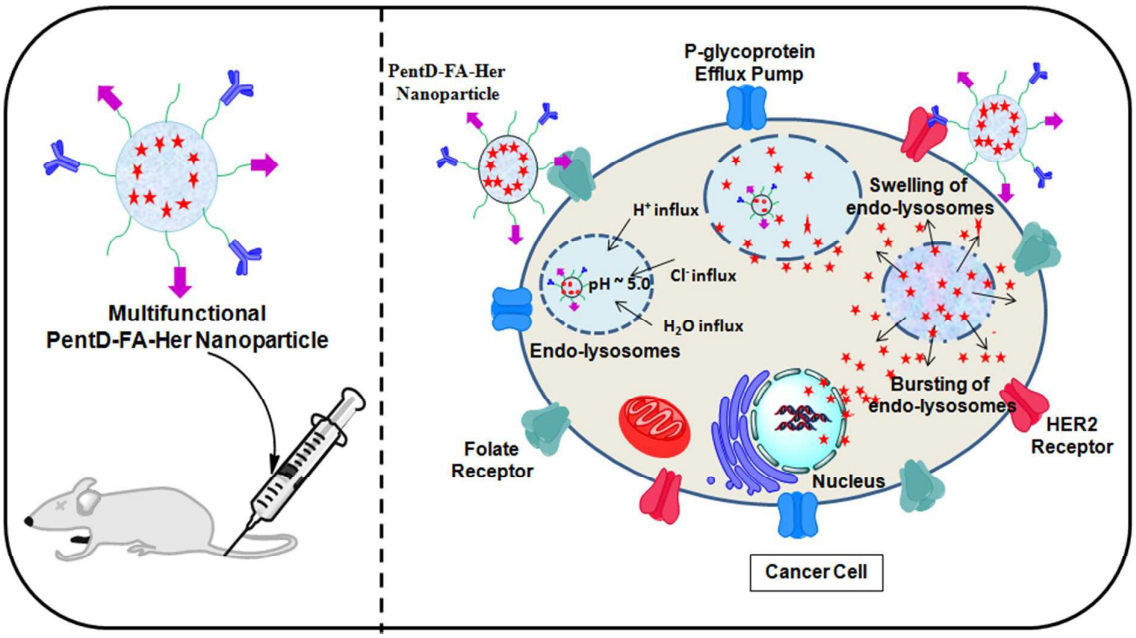

Folic acid and trastuzumab functionalized pH responsive polymeric nanoparticles for intracellular doxorubicin delivery in breast cancer

8 × 4 cm graphical abstract